Renewable Energy 188 (2022) 240–255

Contents lists available at ScienceDirect

Renewable Energy

journal homepage: www.elsevier.com/locate/renene

Catalytic hydrocracking reactions of tetralin biomass tar model compound to benzene, toluene and xylenes (BTX) over metal-modified ZSM-5 in ambient pressure reactor

Andrii Kostyniuk [a, *], David Bajec [a], Blaž Likozar [a, b, c, **]

[a] Department of Catalysis and Chemical Reaction Engineering, National Institute of Chemistry, 19, Hajdrihova, 1001, Ljubljana, Slovenia
[b] Pulp and Paper Institute, 8, Bogišićeva, 1000, Ljubljana, Slovenia
[c] Faculty of Polymer Technology, 19, Ozare, 2380, Slovenj Gradec, Slovenia

ARTICLE INFO

Article history:
Received 24 November 2021
Received in revised form
12 January 2022
Accepted 23 January 2022
Available online 14 February 2022

Keywords:
Catalytic hydrocracking reactions
Ring opening mechanism
Model biomass tar
Benzene/toluene/xylenes (BTX)
Metal-doped HZSM-5 zeolite material
Deposited coke deactivation

ABSTRACT

The tetralin hydrocracking process into benzene, toluene, and xylenes (BTX) was investigated over metal-modified (Ga, Nb, Ni, NiMo, Sn, W, Zr or $H_3[P(W_3O_{10})_4]$)/ZSM-5 zeolite catalysts without sulfidation procedures, mechanism was analyzed, and compared with a pristine microporous material in a packed bed reactor under applied atmospheric pressure (p). This experimental study presents an investigation of the metal-promoted ZSM-5 for the BTX production under the ambient p for the first continuously-operated time. It is demonstrated that metal-wise there are no significant improvements in the formation of BTX. The yield of 43.1 mol% towards BTX over the parent HZSM-5 ($SiO_2/Al_2O_3 = 30$) at 420 °C after 4 h on time on stream (TOS) was achieved, while methane, ethylene, ethane, propylene and propane were main gas products. The outstanding functional performance of HZSM-5 was mainly ascribed to structure, its high dealkylation and a measured large amount of the solid surface area in tandem with the porosity, protonating total Brønsted (BAS)/Lewis (LAS) acidity and BAS/LAS ratio. However, BTX dropped drastically with increasing TOS due to coke. It was found that HZSM-5 was the most affected within studied reaction conditions, but could be easily regenerated with preserving realistic catalytic chemistry. The pathway of cracking was proposed. Simultaneously, the 5wt%Zr/ZSM-5 catalyst possessed the highest selectivity ($S_{BTX} = 24.2$ mol%; TOS = 25 h; 370 °C) due to the low diffusion thermomigration of the Zr species into framework compared to parent zeolite under the same reaction conditions after a long TOS. Influence of metal loading on the activity of ZSM-5 zeolite was systematically studied and the complex relationship between physicochemical properties and catalytic activity of bifunctional catalysts was observed. All these findings shed light, on how the incorporation of different metals affects BTX selectivity.

1. Introduction

Nowadays, humankind obtains 85% of energy from fossil fuels. Even a larger percentage of chemicals is produced from fossil sources, while the development of renewable energy is needed for a sustainable, resource-efficient, and low-carbon economy [1,2]. Hydrogen and carbon are necessary elements for the production of chemicals, where the first one can be obtained from H_2O and the second one from biomass and/or CO_2. Lignocellulosic biomass, which is composed of cellulose (40–50%), hemicellulose (20–35%), and lignin (15–25%), is a renewable source for chemical production (syngas, liquid biofuels, and biochar), which can be utilized via gasification process where the latter has more advantages than pyrolysis or direct combustion [3,4].

Tetralin (tetrahydronaphthalene) has been frequently utilized to represent aromatics in diesel fuel [5] but at the same time, it can represent biomass tar as a model compound [6]. The major part of biomass tar includes naphthalene where the latter can be hydrogenated into tetralin. The direct hydrocracking of naphthalene to BTX is more attractive, but its implementation is not realistic under

* Corresponding author.
** Corresponding author.Department of Catalysis and Chemical Reaction Engineering, National Institute of Chemistry, 19, Hajdrihova, 1001, Ljubljana, Slovenia
E-mail addresses: Andrii.Kostyniuk@ki.si (A. Kostyniuk), blaz.likozar@ki.si (B. Likozar).

https://doi.org/10.1016/j.renene.2022.01.090

ambient pressure and at a mild reaction temperature. Our literature review analysis shows that there are no such studies. Most research groups utilized high pressure (3–10 MPa) [7–9] or high reaction temperature (600–900 °C) but for syngas products [10–12]. Moreover, our recent studies confirmed this assumption, where naphthalene and 1-methylnaphthalene feedstock mixture was utilized [13–15]. It was shown that isomerization, overcracking, and alkylation are the main reactions, while disproportionation, hydrogenation, condensation, and ring opening occurred as side reactions. The only trace amount of BTX was detected.

One of the most promising ways to convert tetralin into high value-added products is hydrocracking into benzene, toluene, and xylenes (BTX), which play an essential role in human modern life with application in the production of fine chemicals, polymers, and petrochemicals [6]. According to the official report [16], the global BTX market is constantly growing and should reach 274.8 billion dollars by 2027 compared to 162.7 billion dollars in 2018, while the largest part of BTX products is derived from non-renewable petroleum-based resources [17]. Commonly, this reaction is carried out under high pressure (10–85 bar), while all the studies under atmospheric pressure, according to our knowledge, are very limited [6] and/or utilize another model compound [13–15].

The pristine and especially metal(s)-modified ZSM-5 catalysts attracted significant attention from both academic and industrial researchers due to their ability to catalyze plenty of different reactions, where ZSM-5 has been often a catalyst of choice for achieving the highest yield of aromatics with various feedstock [18,19]. The catalyst activity depends on the nature of metals and supports that is why unraveling structure-activity relationships and enhancing catalyst design are important research targets for the scientific community involved in heterogeneous catalysis. Table 1 shows that the current research on tetralin hydrocracking to BTX products mainly focuses on the use of various zeolite-supported catalysts at high pressures [20–24]. For instance, Laredo et al. [21,25] studied tetralin hydrocracking over Ni, Mo, W, NiW, CoMo, NiMo, NiSn/Beta, and/or ZSM-5 zeolite catalysts in a bench-scale-trickle-bed reactor at 450–500 °C, 3.9–5.9 MPa, LHSV = 1.3 h^{-1}, and H_2/feed volume ratio = 168–267 m^3/m^3. It was shown that H-ZSM-5 zeolite possesses the highest activity compared to the other studied catalysts (BTX yield = 58 wt%) because of a proper balance between accessible and well-dispersed strong Brønsted acid sites (BAS), but simultaneously a significant catalyst deactivation was observed due to occurrence of polymerization reactions. Nakajima and coworkers [24] found that BEA and MFI zeolites possess relatively high selectivity to butylbenzene and benzene in the reaction of tetralin hydrocracking in a fixed-bed flow reactor at 550 °C under a total pressure of 4 MPa. The highest BTX yield (≈21%) was observed over BEA zeolite which was assigned to the strong BAS and micropore size in the 12-ring pore structure. Besides, the Lee group [23,26] studied selective tetralin hydrocracking into BTX over various metallic components (Ni, NiSn, NiW–S, CoMo–S, and NiMo–S) on H-Beta zeolite support in tandem with H-ZSM-5 in the physical mixture in a fixed-bed down-flow reactor at 4 MPa. It was shown that the NiMo–S/HZSM-5 (10 wt%)/Beta catalyst is the most active with achieved BTX yield = 54.3 wt% at 425 °C. This high catalyst activity was attributed to its high acidity and small pore size. It was demonstrated that the addition of H-ZSM-5 zeolite to NiMo–S/Beta increased BTX yield due to the high dealkylation activity of the 10-ring pore structure of H-ZSM-5, which facilitates the conversion of alkylbenzenes into BTX.

In Table 1, it can be seen that many researchers tried to convert biomass tar and/or its model compounds into high value-added chemicals such as BTX but only under high pressure. It can be observed that only Bi et al. [27] studied biomass tar conversion into BTX under ambient pressure but using a combination of H-ZSM-5 zeolite catalyst and current-enhanced catalytic conversion (CECC). According to our knowledge, other research groups applied high pressure (3–10 MPa), while our reaction was conducted under atmospheric pressure. It is well known that conducting reactions at the atmospheric pressure has more advantages than under high pressure due to lower operational costs and simplified reactor maintenance (Fig. S1).

The present work was performed during the CONVERGE (Carbon Valorisation in Energy-Efficient Green Fuels) Horizon 2020 project (EU funding program for research and innovation) where the MILENA gasifier is modified and combined with the most active catalyst, which will allow a significant reduction of heavy-tars out from secondary waste biomass. CONVERGE will progress the technology beyond the state-of-the-art by targeting only the components larger than C_9 and by directing this energy content into BTX. By converting the energy in tar into the energy in BTX, the amount of BTX can be doubled in the process. In this case, the

Table 1
Conversion of biomass tar or its model compounds over zeolite and metal-promoted zeolite catalysts.

Catalyst	SiO_2/Al_2O_3	Model compounds or tar	T, °C	Pressure, MPa	Conversion (%)	Products	Refs
ZSM-5	50	biomass tar	400	Atmospheric + CECC	27.0	BTX (25.1%)	[27]
Ni_2P/Beta	25	5 wt% naphthalene, tridecane	400	3.0	99.0	BTX (94.4%)	[8]
NiMoS–Al_2O_3-coated/USY(50 wt%)	30	1-methylnaphthalene	360	5.0	100	(alkyl)benzenes (53.5%) + BTX (37.7%)	[28]
NiW-TBOS/silylated-Beta	38	1-methylnaphalene	400	5.0	97	ring opening yield (58.5%)	[29]
$Ni_{1.1}W$/Beta	38	1-methylnaphalene	400	5.0	97	BTEX (39.6%)	[30]
Ni_2P/Beta	25	1-methylnaphtalene + 15 wt% phenanthrene	380	6.0	95.0	BTX (42.3%)	[31]
25%W/Beta	50	1-methylnaphalene	420	6.0	100	BTX (53.0%)	[32]
NiMo/Beta	37	10 wt% 1-methylnaphthalene + 0.1 wt% dibenzothiophene in decalin	360	5.0	96	BTX (N/A)	[33]
NiSn/Beta	38 or 75	tetralin	450	4.0	99.5	BTX (48.1%)	[20]
NiMo–S/ZSM-5 (10 wt%)/Beta	30; 38 or 75	tetralin	425	4.0	97.6	BTX (54.3%)	[23]
CoMo/Beta	25	tetralin	370	8.0	99.5	BTX (54.2%)	[22]
		pyrolysis fuel oil			70.0	BTX (31.3%)	
NiW/HY(meso)	–	phenanthrene	375	10.0	99.9	BTEX (48.4%)	[34]
ZSM-5	50	tetralin	500	4.9	99.7	BTX (58%)	[21,25]
Beta		tetralin	550	4.0	82.0	BTX (21%)	[24]

overall efficiency is increased, since no energy is lost. BTX recovery in biomass gasification is not practiced commercially and does not currently exist as a topic.

In our recent work [6], we found a superior activity of the H-ZSM-5 zeolite for tetralin conversion into BTX products compared to the H-Beta, H-Mordenite, H-USY, and H−Y zeolites in a packed bed reactor under ambient pressure. This high activity was attributed to the presence of the high mesopore volume and mesopore surface area, the mild acidity, and the highest Brønsted to Lewis acid sites ratio (BAS/LAS) in the H-ZSM-5 catalyst. These findings stimulated us to continue our investigations and to select the H-ZSM-5 catalyst for our further experimental studies. This work aims to elucidate the H-ZSM-5 catalyst behavior more deeply and to study the effect of metal(s) promoters without sulfidation procedures on its catalytic activity and stability in the reaction of tetralin conversion into BTX products under atmospheric pressure. Herein, we demonstrate that the nature and density of acid sites in H-ZSM-5 impregnated by different metals could shift the product distribution in a reaction of tetralin hydrocracking into BTX. It has been shown that the metal modification of H-ZSM-5 parent zeolite (excluding 5%Zr/ZSM-5) leads to a decrease in catalytic activity. The influence of metal loading on ZSM-5 support was systematically investigated and the relationship between physicochemical properties of catalysts and catalytic activity was presented. The catalysts morphology, structure, texture, and acidity were characterized by X-ray diffraction analysis (XRD), N_2 physisorption, inductively coupled plasma with optical emission spectrometry (ICP-OES), temperature-programmed desorption of ammonia (NH_3-TPD), and pyridine diffuse reflectance infrared Fourier transform spectroscopy (Pyridine-DRIFTS). Finally, plausible reaction pathways for the production of BTX were proposed based on the collected analytical data. To the best of our knowledge, such systematic studies of synthesized catalysts with their evaluation performance in BTX production from tetralin under ambient pressure have not been reported in the literature.

2. Experimental section

2.1. Chemicals used and catalysts preparation

Reagents that were purchased from commercial suppliers: H-ZSM-5 ($SiO_2/Al_2O_3 = 30$, Zeolyst International) which was calcined for removing impurities at 550 °C (heating rate of 10 °C/min) in the air for 6 h; H_3 [$P(W_3O_{10})_4$] (Merck, > 99.9%), $ZrO(NO_3)_2 \times 6H_2O$ (Merck, > 99.99%), $Ga(NO_3)_3 \times H_2O$ (Merck, > 99.9%), $Cl_4H_{10}O_5Sn$ (Merck, > 99.9%), $C_{10}H_2Nb_2O_{21}$ (Merck, > 99.9%), $Ni(NO_3)_2 \times 6H_2O$ (Merck, 98.5+%), $(NH_4)_6Mo_7O_{24} \times 4H_2O$ (Merck, 99.98%), and $(NH_4)_6W_7O_{24} \times 4H_2O$ (Merck, 66.5%).

Gases and external calibration standards that were utilized: hydrogen (5.0, Messer, Bad Soden am Taunus, Germany), nitrogen (5.0, Messer, Bad Soden am Taunus, Germany), NH_3 (10 vol% in He, Linde, Pullach, Germany), helium (5.0, Messer, Bad Soden am Taunus, Germany), air (5.0, Messer, Bad Soden am Taunus, Germany), tetralin (Alfa Aesar, 97%), ethylbenzene (Alfa Aesar, 99%), benzene (Merck, 99.8%), toluene (Merck, 99.8%), m-xylene (Merck, 99%), o-xylene (Merck, 97%), p-xylene (Merck, 99%), naphthalene (Merck, 99%), 1-methylnaphthalene (Merck, 95%), 2-methylnaphthalene (Merck, 97%), phenanthrene (Merck, 98%), anthracene (Merck, 97%), indane (Alfa Aesar, 95%).

The preparation of the 5wt%Zr/ZSM-5, 20wt%Zr/ZSM-5, 5wt% Nb/ZSM-5, 5wt%Sn/ZSM-5, 5wt%Ga/ZSM-5, 5wt%Ni/ZSM-5, 2.5wt% Ni2.5wt%Mo/ZSM-5, and 20wt%W/ZSM-5 catalysts involved the impregnation of H-ZSM-5 zeolite using the wet impregnation method with an aqueous solution of 0.01 M $ZrO(NO_3)_2 \times 6H_2O$, $C_{10}H_2Nb_2O_{21}$, $Cl_4H_{10}O_5Sn$, $Ga(NO_3)_3 \times H_2O$, $Ni(NO_3)_2 \times 6H_2O$, $(NH_4)_6Mo_7O_{24} \times 4H_2O$, and $(NH_4)_6W_7O_{24} \times 4H_2O$, respectively. Briefly, corresponding salt solutions were added to the H-ZSM-5 zeolite with vigorous stirring for 4 h at 80 °C. Thereafter, all the samples were dried overnight at 110 °C. Afterward, the samples were calcined for 6 h at 550 °C.

In the case of the 20wt%$H_3[P(W_3O_{10})_4]$/ZSM-5 (HPA/ZSM-5) catalyst preparation the Keggin-type phosphotungstic acid was loaded on zeolite support through incipient wetness impregnation method following the procedure similar to works [35–37]. HPA/ZSM-5 catalyst was prepared by the incipient wetness method with an ethanol solution at room temperature. HPA was used as reference material and dried overnight at 100 °C. To prepare HPA/ZSM-5, 1.0 g of HPA was dissolved in 50 ml of ethanol and impregnated to the ZSM-5 zeolite support with HPA loading of 20 wt%. Following, the sample was kept at room temperature for 24 h under constant stirring to reach a uniform distribution of HPA clusters onto the metal modified zeolite and then dried in an oven at 110 °C overnight. Before use, the synthesized HPA/ZSM-5 catalyst was calcined at 400 °C for 3 h in an air flow.

2.2. Catalyst characterization

The element content was determined by inductively coupled plasma optical emission spectroscopy (ICP-OES) using a PerkinElmer Optima 8000. Before the analysis, the samples were dissolved in 2.0 cm^3 HF, 3.0 cm^3 HNO_3, and 3.0 cm^3 HCl and diluted to obtain aqueous solutions which also contained 12.0 cm^3 H_3BO_4 for complexation of excessive HF.

N_2 physisorption measurements were conducted using a Tristar 3000 (Micromeritics, Communications Drive Norcross, GA, USA). The samples (0.15 g) were degassed in a vacuum and heated to 200 °C overnight. The specific surface area was calculated from adsorption data in the relative pressure range from 0.06 to 0.30 applying the Brunauer-Emmett-Teller (BET) method. The total pore volume was estimated based on the amount of adsorbed nitrogen at the relative pressure of 0.989. Pore size distributions were calculated based on the Barrett-Joyner-Halenda (BJH) method for desorption.

X-ray diffraction (XRD) patterns of catalysts were recorded on a PANalytical Xpert PRO MPD, Malvern PANalytical, Worchestershire, UK, using CuKα1 radiation (1.5406 Å) in 2 theta range 4–90° with increments of 0.034° at room temperature with the tube voltage and current of 40 kV and 40 mA, respectively. Scanning electron microscopy (SEM) was performed on Zeiss Supra TM 35 VP (Carl Zeiss AG, Oberkochen, Germany). The Match! 2.0 software with the data from the Crystallography Open Database (COD) was used to determine the crystalline phases, while the Scherrer equation was applied to estimate the crystallite sizes of the synthesized catalysts.

The temperature-programmed desorption of ammonia measurements was performed in a Micromeritics Autochem 2920 II instrument equipped with a Pfeiffer Vacuum Thermostar quadrupole mass spectrometer for the detection of desorbed NH_3 gas with $m/z = 15$. When the experiment (NH_3 desorption) was finished the calibration of MS was conducted with at least 5 pulses of NH_3 and a known concentration of the latter for the quantification of the surface acidity of the selected catalysts. Pyridine-DRIFTS analysis was used to determine the density of BAS and LAS of the synthesized catalyst using a Frontier IR spectrometer (PerkinElmer), DiffusIR® accessory from Pike Scientific. Briefly, the DRIFTS spectra were recorded in the range of 800–4000 cm^{-1} by collecting 64 scans at 4 cm^{-1} resolution using a diffuse reflectance cell and a mercury cadmium telluride (MCT) detector cooled by liquid N_2. The catalyst samples were loaded into the cell and treated under N_2 flow (50 ml/min) at 400 °C for 1 h under vacuum conditions (2×10^{-3} mbar), and then the samples were cooled down to 125 °C

and the background spectrum was collected before the start of pyridine adsorption with the following spectra transformation into the Kubelka-Munk units. More experimental details about carrying out the NH_3-TPD-MS and Pyridine-DRIFTS analyses have been presented in our recently published works [6,13]. Finally, the amount of coke was quantified for the spent catalysts via total carbon (TC) analysis using Rosemount Analytical Dohrmann DC−190.

2.3. Catalytic activity

The experimental setup for the hydrocracking of tetralin and its detailed description is presented in our recently published study [6]. Briefly, the reaction was carried out in a continuous flow fixed-bed microactivity reactor system (Microactivity-Reference, PID Eng&Tech). The reactor is a tube (9 mm internal diameter and 305 mm long) made from stainless steel inside of which 0.5 g of catalyst was loaded and stabilized with glass wool on both sides. Before the reaction, the catalyst was pretreated under hydrogen flow (150 ml/min) at 370 °C for 2 h. Tetralin was fed into the hot box which was heated up to 140 °C by using 307 HPLC Piston Pump (Gilson Inc.). Thereafter, the gas mixture of tetralin and H_2 was introduced into the packed-bed reactor. The flow of H_2 was controlled by Brooks mass flow controllers. The activity tests were conducted at the following conditions: $WHSV_{Tetralin} = 2\ h^{-1}$; $GHSV_{total} = 980\ h^{-1}$; H_2/Tetralin = 1800 (volume ratio); P = 1 bar for 24 h in the temperature range of 370–420 °C measured by a K-type thermocouple. At first, the liquid product was collected from the Peltier cell and cooled down at 0 °C, and thereafter accumulated in the second condenser. The gas products were separated and analyzed online on micro GC Fusion Inficon equipped with Rt-Molsieve 5A, Rt-Q-BOND, and Rt-U-BOND capillary columns and two thermal conductivity detectors (TCD).

The collected liquid product was analyzed offline using a gas chromatography GC (Thermo Scientific FOCUS) with capillary column Zebron ZB-5 Phenomenex (60 m × 0.25 mm × 0.25 μm) fitted with a flame ionization detector (FID). Liquid products were identified and quantified using an external calibration method and verified by a gas chromatography-mass spectrometry system (Shimadzu, GC/MS-QP2010) with the Zebron TM ZB-5MS capillary column (60 m × 0.25 mm × 0.25 μm).

All liquid and gas products were calibrated over a wide range of concentrations. The conversion of tetralin, $X_{Tetralin}$, was calculated using the next equation:

$$X_{Tetralin}(mol\%) = \frac{n(\text{Tetralin})_{in} - n(\text{Tetralin})_{out}}{n(\text{Tetralin})_{in}} \times 100 \quad (1)$$

The selectivity of BTX, S_{BTX}, and its yield, Y_{BTX}, calculated using the equations below:

$$S_{BTX}(mol\%) = \frac{n(\text{BTX})}{n(\text{Tetralin})_{in} - n(\text{Tetralin})_{out}} \times \frac{Z_i}{Z_{Tetralin}} \times 100 \quad (2)$$

$$Y_{BTX}(mol\%) = \frac{n(BTX)}{n(\text{Tetralin})_{in}} \times \frac{Z_i}{Z_{Tetralin}} \times 100 \quad (3)$$

where n $(\text{Tetralin})_{in}$ and n $(\text{Tetralin})_{out}$ are the input and output moles of tetralin before and after reaction, respectively; n (BTX) is the sum of moles of benzene, toluene, and xylenes; Z_i and $Z_{Tetralin}$ are the number of carbon atoms in the products and tetralin, respectively.

The values in this manuscript are in mole percent. The experimental error was established based on the three times experiment and it was no more than 2% for all identified liquid and gas products. The carbon mass balance was determined in the range of 98–100% for all the catalyst tests.

3. Results and discussion

3.1. Catalysts characterizations

Structural, textural, and morphological properties together with the chemical composition were carried out using a variety of characterization techniques including ICP-OES, N_2 physisorption, XRD, NH_3-TPD, and pyridine-DRIFTS measurements. The N_2 adsorption-desorption isotherms and pore-size distributions are presented in Fig. 1, while the BET surface area (including micropore and mesopore), pore volume (total, micropore, and mesopore), average pore diameter, relative crystallinity, average crystallite size, and hierarchy factor (HF) are summarized in Table 2. ICP-OES measurements indicate the amount of metal(s) loadings that are close to the theoretical values, excluding 14.5 wt% of W, where the discrepancy can be explained by the experimental error during the catalyst preparation.

The N_2 adsorption-desorption isotherms for all the studied catalysts show type IV isotherm with H4 type hysteresis loop at the high relative pressure (P/P_0 = 0.45–1.0) region (Fig. 1S and a), which indicates the presence of both micro- and mesoporous structures due to the adsorption of N_2 on the external surface of the crystallites and capillary condensation in the spaces between the crystallites according to International Union of Pure and Applied Chemistry (IUPAC) classification [38,39]. The loading of metal(s) and HPA to H-ZSM-5 led to a decrease of adsorbed N_2 quantity and

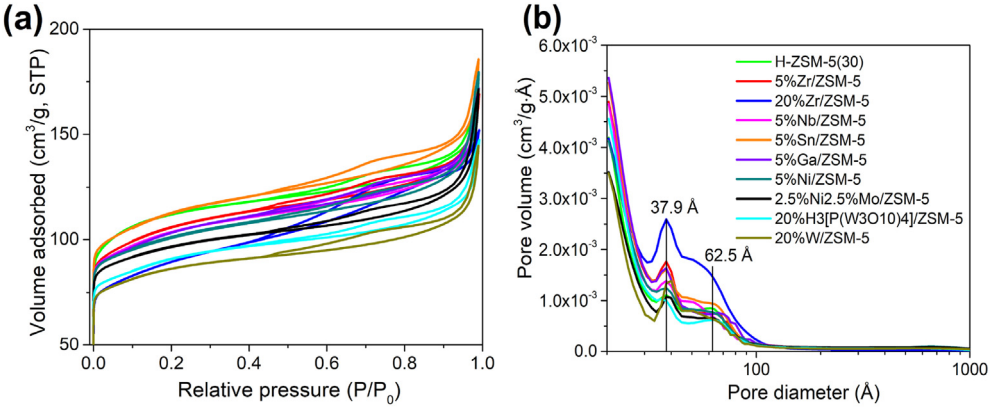

Fig. 1. N_2 adsorption-desorption isotherms (a) and pore-size distributions (b) of H-ZSM-5 and metal(s)-modified zeolite catalysts.

Table 2
Chemical analysis and structural properties of the various zeolite catalysts.

Catalyst	Metal(s) content (wt.%)	S_{BET}[b] (m^2/g)	S_{micro}[b] (m^2/g)	S_{meso}[b] (m^2/g)	V_{micro}[c] (cm^3/g)	V_{total}[c] (cm^3/g)	V_{meso}[c] (cm^3/g)	PD[d] (Å)	HF[e]	Average crystallite size[f] (nm)	Relative crystallinity[f] (%)
HZSM-5	–	348	230	118	0.12	0.25	0.13	64	0.16	50.3	100
5%Zr/ZSM-5	4.8	313	177	136	0.10	0.25	0.15	59	0.17	51.1	94.5
20%Zr/ZSM-5	17.6	271	133	138	0.08	0.23	0.15	50	0.18	49.4	67.3
5%Nb/ZSM-5	4.5	306	175	131	0.10	0.25	0.15	63	0.17	51.7	88.7
5%Sn/ZSM-5	4.8	333	189	144	0.11	0.27	0.16	63	0.18	51.4	68.4
5%Ga/ZSM-5	4.8	308	166	142	0.10	0.25	0.15	61	0.18	50.8	100.7
5%Ni/ZSM-5	4.6	315	198	117	0.10	0.26	0.16	74	0.15	46.3	84.9
2.5%Ni2.5%Mo/ZSM-5	2.3; 2.3	300	200	100	0.11	0.26	0.15	81	0.14	46.5	76.9
20%$H_3[P(W_3O_{10})_4]$/ZSM-5	–	260	143	117	0.09	0.22	0.13	63	0.18	51.8	85.1
20%W/ZSM-5	14.5	268	170	98	0.09	0.21	0.12	72	0.16	41.9	71.3

[a]Metal(s) content according to ICP-OES.
[b] BET method.
[c] t-plot method.
[d] Average pore diameter measured from the desorption branch according to the BJH method.
[e] $HF = (S_{meso}/S_{BET}) \times (V_{micro}/V_{total})$.
[f] The crystallite size and relative crystallinity were calculated from the seven most intensive diffraction peaks of XRD spectra. Results were normalized to the commercial HZSM-5 catalyst [42].

BET specific surface area (from 348 to 260 m^2/g) possibly due to the covering and/or blocking of pores in the zeolite support. The H-ZSM-5 zeolite had the highest surface area of 348 m^2/g. Simultaneously, it can be seen that 5%Sn/ZSM-5, 5%Ni/ZSM-5, and 5%Zr/ZSM-5 catalysts possess the surface areas (333, 315, and 311 m^2/g, respectively) close to the H-ZSM-5 which indicates that metal particles are finely dispersed and incorporated on/into the support [40]. Importantly, after the metal impregnation the mesopore surface area (S_{meso}) increased for 5%Zr/ZSM-5 (136 m^2/g), 20%Zr/ZSM-5 (138 m^2/g), 5%Ga/ZSM-5 (142 m^2/g), 5%Sn/ZSM-5 (144 m^2/g) catalysts, whereas the micropore surface area (S_{micro}) decreased for all the studied promoted catalysts in comparison to the parent zeolite. The total pore volume (V_{total}) was in the range of 0.21–0.27 cm^3/g, while the mesopore volume (V_{meso}) increased after the introduction of metals for all the samples (excluding HPA and W) and was within 0.14–0.16 cm^3/g. HF was higher than 0.10 for all the studied catalysts and even higher than 0.15 (excluding 2.5%Ni2.5%Mo/ZSM-5 and 5%Ni/ZSM-5) which revealed the presence of hierarchical (mesoporous) zeolite structure.

Fig. 1b represents the pore size distribution of H-ZSM-5 and metal(s)-modified zeolite catalysts measured by the BJH method. The mesopores distribution for all the studied samples was centered approximately at 30–45 Å and 45–100 Å, which indicates the three-gradient porous structure [41]. According to HRSEM results from our previous studies [6,13,14], we can assume that the average particle size of the studied catalysts is located in the range of 100–200 nm.

Fig. 2 presents the XRD patterns of the commercial and metal(s)-modified zeolite catalysts. All of the synthesized samples showed the characteristic diffraction peaks related to well-crystallized MFI structure (JCPDS 42–0024) at 2θ of 7.88°, 8.79°,13.87°, 14.75°, 23.05°, 23.85°, 23.88° and 24.34° [43–46]. It was observed (Fig. 2b) that the characteristic peaks at 2θ of 7.91°and 8.79° that refer to the (011) and (200) crystal planes, respectively, are increased only for the 5%Ga/ZSM-5 catalyst which is in good agreement with the literature data [47]. This finding indicates that the crystallinity of the support in 5%Ga/ZSM-5 catalyst is even slightly higher (Table 2) than the parent H-ZSM-5 zeolite after the impregnation of $Ga(NO_3)_3$. At the same time, other metal(s)-modified zeolite catalysts show a decrease of the characteristic diffraction peaks in the same 2θ range in comparison to H-ZSM-5 parent zeolite. This might be attributed to the decrease of the relative degree of crystallinity due to the incorporation of metal species on/into zeolite support but without affecting their structure as shown in Fig. 2a [40]. Interestingly, the highest crystallinity (excluding 5%Ga/ZSM-5) was observed over the 5%Zr/ZSM-5 catalyst (94.5%) which indicates that migration of zirconium species into ZSM-5 support was low. In addition, no crystalline diffraction peaks that could be attributed to Ni, Mo, Nb, and Zr species in the 2.5%Ni2.5%Mo/ZSM-5, 5%Nb/ZSM-5, and 5%Zr/ZSM-5 samples were observed, which implies that these metal species exist as highly dispersed extracrystalline oxide at the external zeolite surface and/or dispersed framework or extraframework species [48]. Fig. 2d–f shows that when the metal loading was increased to 20 wt% for the samples 20%W/ZSM-5, 20%HPA/ZSM-5, and 20%Zr/ZSM-5 the peaks related to WO_3 (2θ = 23.66°, 33.53°, 41.35°, 48.28°, 54.20°, 59.88°) and ZrO_2 (2θ = 30.33°, 50.32°, 60.47°) were detected. In addition, the peaks of NiO (37.17°, 43.25°, 62.73°, 75.30°, 79.42°) and SnO (33.89°, 51.89°) were observed (Fig. 2d–f) over the 5%Ni/ZSM-5 and 5%Sn/ZSM-5 catalysts, respectively.

The distribution, quantification of the acid sites, and their properties on metal(s)-modified and pristine zeolite catalysts were investigated by NH_3-TPD (Fig. S3), and the corresponding data are presented in Table 3. As shown in Fig. S3, two obvious NH_3 desorption peaks were detected over all the studied catalysts, which corresponds to the weak acid sites (100–300 °C) attributed to the physisorbed NH_3 desorption, hydrogen bonding, and/or weakly adsorbed NH_3 by the weak LAS (cation-bonded silanol group) and BAS (terminal silanol group), and to the strong acid sites (300–600 °C) with strongly adsorbed NH_3 by the strong BAS (acidic protons at the bridging Si–(OH)–Al sites) and the strong LAS (extra Al framework of the Si–(O)–Al sites), respectively [49,50]. It was found that the high and low desorption peaks for all the studied metal-modified zeolite catalysts are shifted (with regard to H-ZSM-5 at 206.6 and 401.8 °C) to lower temperature which can be explained by the lower intrinsic acidity of BAS as a result of metal(s) species covering of the zeolite support during modification [51]. The desorption peaks of ammonia in the high temperature range were reduced over all the metal-modified zeolites, indicating that the acid sites were covered and/or neutralized by metal(s) species.

The temperature maximum in the range of 318.3–401.8 °C for the strong acid sites was decreased as follows: H-ZSM-5 › 5%Zr/ZSM-5 › 5%Sn/ZSM-5 › 20%W/ZSM-5 › 5%Nb/ZSM-5 › 5%Ga/ZSM-5 › 20%HPA/ZSM-5 › 20%Zr/ZSM-5 › 5%Ni/ZSM-5 › 2.5%Ni2.5%Mo/ZSM-5. While the temperature shifting in the range of 195.7–206.6 °C for the weak acid sites was different and decreased as follows: H-ZSM-

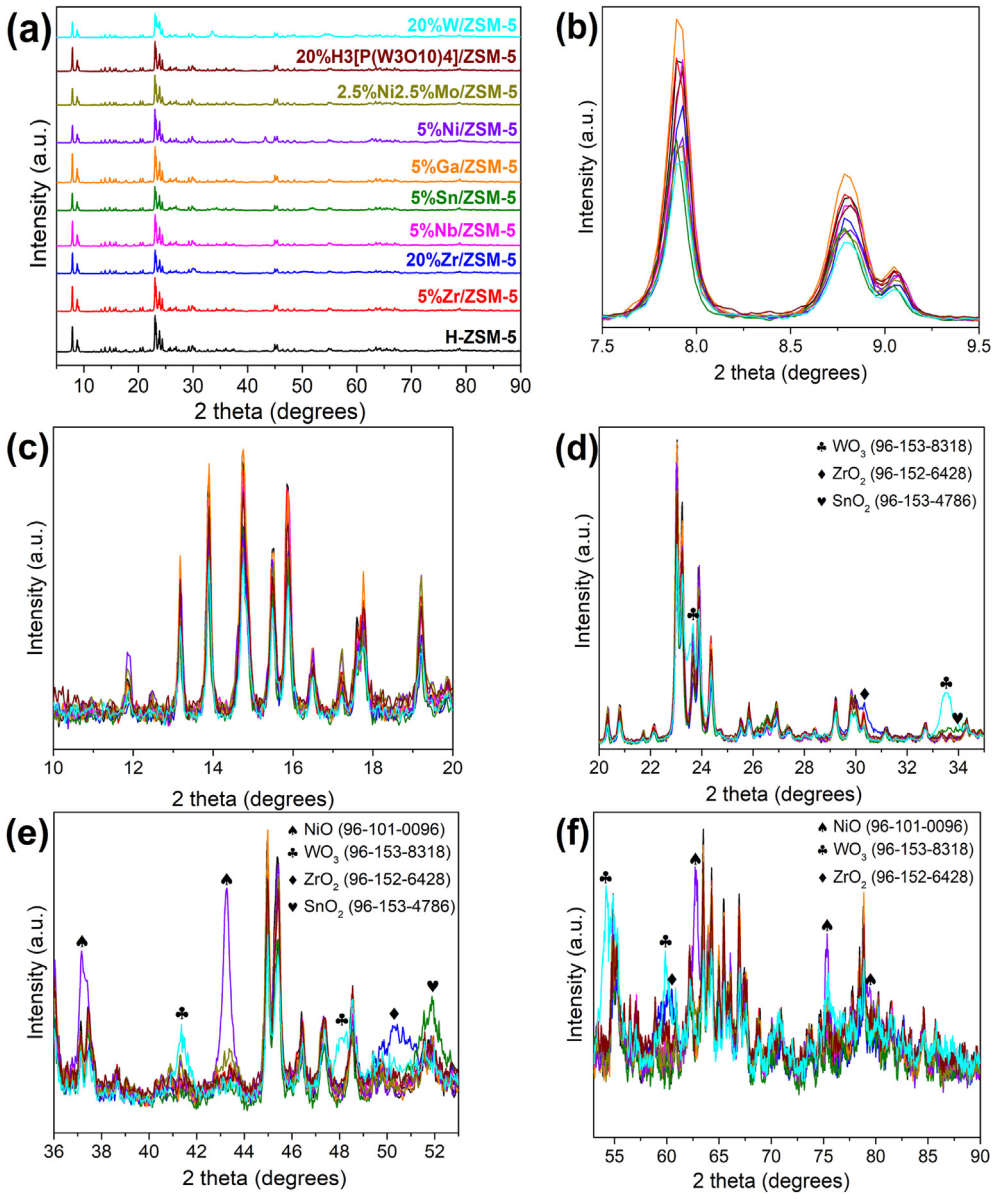

Fig. 2. XRD patterns of the parent and metal-modified ZSM-5 catalysts.

Table 3
Acid properties of the parent and metal(s)-modified ZSM-5 catalysts based on NH_3-TPD and Pyridine-adsorption FTIR analyses.

Catalyst	Acidity by NH_3-TPD ($mmol_{NH3}/g_{cat}$)					Acidity by Pyridine-FTIR ($\mu mol_{pyridine}/g_{cat}$) at 1545 and 1450 cm^{-1}			
	Total	Weak	T (°C)	Strong	T (°C)	BAS	LAS	BAS/LAS ratio	BAS + LAS
H-ZSM-5	1.06	0.60	206.6	0.46	401.8	25.1	8.1	3.1	33.3
5%Zr/ZSM-5	0.95	0.52	203.7	0.43	389.1	6.8	4.3	1.6	11.0
20%Zr/ZSM-5	0.62	0.19	195.7	0.43	334.1	1.5	2.4	0.6	3.9
5%Nb/ZSM-5	0.76	0.26	201.9	0.50	354.3	9.8	3.8	2.6	13.6
5%Sn/ZSM-5	0.76	0.41	200.5	0.35	386.8	9.3	4.0	2.3	13.3
5%Ga/ZSM-5	0.70	0.23	200.8	0.47	348.6	4.3	3.6	1.2	7.8
5%Ni/ZSM-5	0.97	0.30	200.9	0.67	327.3	6.6	8.4	0.8	15.0
2.5%Ni2.5%Mo/ZSM-5	1.04	0.37	198.5	0.67	318.3	11.1	8.4	1.3	19.5
20%$H_3[P(W_3O_{10})_4]$/ZSM-5	0.76	0.27	198.2	0.49	335.0	14.1	4.2	3.3	18.3
20%W/ZSM-5	0.79	0.43	202.8	0.37	357.2	8.5	3.7	2.3	12.2

5 > 5%Zr/ZSM-5 > 20%W/ZSM-5 > 5%Nb/ZSM-5 > 5%Ni/ZSM-5 > 5%Ga/ZSM-5 > 5%Sn/ZSM-5 > 2.5%Ni2.5%Mo/ZSM-5 > 20%HPA/ZSM-5 > 20%Zr/ZSM-5. Interestingly, both H-ZSM-5 and 5%Zr/ZSM-5 catalysts show the highest temperature maximum for the weak and strong acid sites.

All the NH_3-TPD desorption peaks were separated into two Gaussian peaks (Fig. S3) by deconvolution and quantified. Table 3 shows that for all the studied catalysts the total acidity is in the range of 0.62–1.06 $mmol_{NH3}/g_{cat}$. The largest amount of total acidity, including weak and strong acid sites, was detected for the parent H-ZSM-5 catalyst, which is in agreement with pyridine-DRIFTS results. The order of total acidity decreasing follows the trend: H-ZSM-5 > 2.5%Ni2.5%Mo/ZSM-5 > 5%Ni/ZSM-5 > 5%Zr/ZSM-5 > 20%W/ZSM-5 > 20%HPA/ZSM-5 ≥ 5%Sn/ZSM-5 ≥ 5%Nb/ZSM-5 > 5%Ga/ZSM-5 > 20%Zr/ZSM-5.

In order to evaluate the amount and type of acid sites, the Pyridine-DRIFTS analyses were carried out and are presented in Fig. 3. According to the literature [14,52,53], the band areas adsorbed at 1450 and 1545 cm^{-1} are related to the concentration of LAS and BAS, respectively. The peak at 1491 cm^{-1} is assigned to both BAS and LAS, while 1614 and 1602 cm^{-1} correspond to LAS [54,55]. The band at 1638 cm^{-1} attributed to the vibrations of pyridine adsorbed on BAS [53,56]. Also, we can suppose that the ring stretching modes of physically adsorbed and hydrogen-bonded pyridine appear as a shoulder or in an overlapping form with LAS and can be presented at 1597 cm^{-1} after deconvolution [57]. The total concentration of BAS and LAS were calculated using the integrated molar extinction coefficients (ε(B) = 1.67 cm/μmol and ε(B) = 2.22 cm/μmol) determined by Emeis [58].

Results show that the H-ZSM-5 catalyst possesses the highest amount of BAS and total acid sites among all the studied catalysts, while LAS density is significantly higher for 2.5%Ni2.5%Mo/ZSM-5 and 5%Ni/ZSM-5 catalysts which include an additional amount of strong LAS which is also correlated with our previous studies [13,14]. The impregnation of metal(s) species leads to dealumination of the zeolite framework with the production of extra-framework alumina, thus stimulating a decrease of BAS and increase of LAS [59]. An additional factor is the ion-exchange with metals, which also can modify the SiO_2/Al_2O_3 ratio of zeolite and decrease BAS. Unfortunately, there is no perfect correlation between NH_3-TPD and pyridine-DRIFTS results. We would like to stress that all samples were analyzed at least 3 times and the good fit between NH_3-TPD and pyridine-DRIFTS data was not observed. The reason for this mismatch can be attributed to the steric hindrance of pyridine. It is known that pyridine can interact with the acid sites in the main channels of zeolite but not with those inside the smaller side pockets, while NH_3 molecules interact with more acid sites in the pore system [60]. Furthermore, the straightforward correlation between BAS and reactivity is limited to zeolites with MFI and CHA topology [61].

According to recent studies by Wang et al. [50], the protonic sites of H-ZSM-5 catalyst can be neutralized by metal species (or metal clusters after its reassembling) with high thermomigration ability after metal(s) impregnation or physical mixing method through a solid ion-exchange mechanism, which can lead to a significant drop of catalytic activity due to block and cover the micropore of zeolite and neutralization of BAS. Simultaneously, the authors established that Zr species possessed the lowest thermomigration ability which resulted in a high catalytic performance in the selective CO_2 hydrogenation reaction into C_{2+} hydrocarbons. Therefore, we speculate that this unique behavior of the Zr/ZSM-5 bifunctional catalyst, with no visible metal species migration, can occurre in our case too. Indeed, the 5%Zr/ZSM-5 exhibited the highest stability and BTX selectivty (after TOS = 25 h) compared to the other studied catalyst samples (see below). Thus, these observations demonstrate that the dispersed Zr species on the surface of ZSM-5 support has a promotion effect on the hydrocracking of tetralin into BTX even with lower acidity in comparison to the pristine zeolite.

3.2. Catalytic performance

We compared the catalytic performance of tetralin hydrocracking over the pristine and metal(s)-modified bifunctional catalysts under mild reaction conditions at 370 °C and ambient pressure. As an example of the observed product, the GC-FID product distribution over the 20%W/ZSM-5 catalyst is displayed in Fig. S4. It has been confirmed that BTX products can be formed under atmospheric pressure in the temperature range of 320–420 °C.

Fig. 4a shows that BTX selectivity after TOS = 4 h decreases as follows: H-ZSM-5 > 5%Zr/ZSM-5 > 5%Nb/ZSM-5 > 20%W/ZSM-5 > 5%Ni/ZSM-5 > 20%Zr/ZSM-5 ≈ 20%$H_3[P(W_3O_{10})_4]$/ZSM-5 ≈ 5%Sn/ZSM-5 > 5%Ga/ZSM-5 > 2.5%Ni2.5%Mo/ZSM-5. It was not found the perfect correlation between catalysts acidity and BTX selectivity. This difference can be explained by the combination of complex factors (differences in textural, morphological, acid, and redox properties) which can influence the catalytic activity. Interestingly,

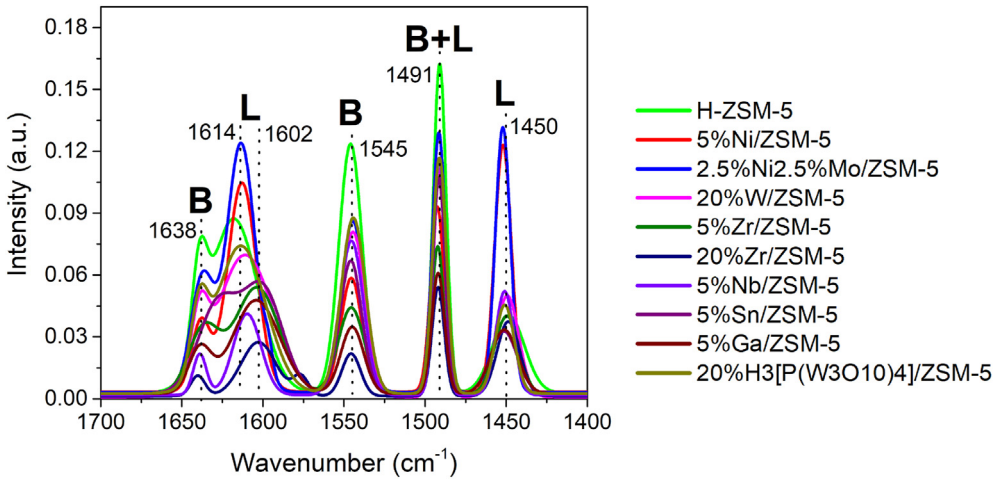

Fig. 3. Pyridine-adsorption FTIR spectra of the parent and metal(s)-modified ZSM-5 catalysts after adsorption on Brønsted (B) and Lewis (L) acid sites.

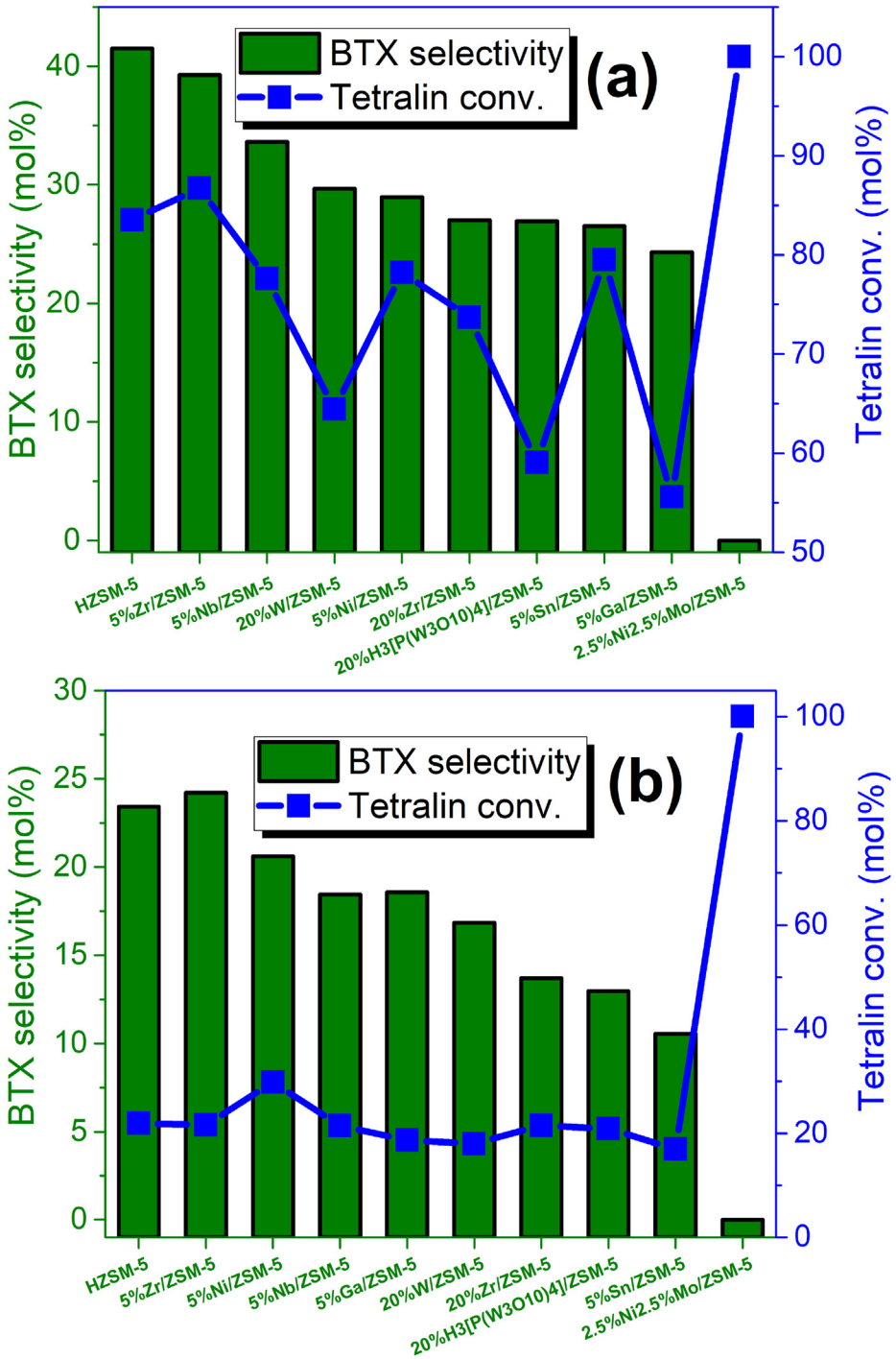

Fig. 4. Tetralin conversion and BTX selectivity over pristine HZSM-5 and metal(s)-modified catalysts with TOS = 4 h – (a) and TOS = 25 h – (b). Rxn conditions: catalyst, 0.5 g; $T_{reactor}$ = 370 °C; H_2 carrier gas; $WHSV_{Tetralin}$ = 2 h^{-1}; $GHSV_{total}$ = 980 h^{-1}; H_2/Tetralin = 1800 (volume ratio); P = 1 bar.

very recently Laredo et al. [25] presented a comparison of the literature results with their own, where a similar superior activity of ZSM-5 (BTX total yield = 58.7 wt%) among various zeolites (H-Beta, H–Y) and metal(s)-modified (Mo, Ni, Co, W, CoMo, NiSn, NiW, NiMo) zeolite catalysts was achieved. The authors [21] obtained this remarkable BTX yield after tetralin hydrocracking in a bench-scale-trickle-bed reactor at 500 °C, P = 4.9 MPa, LHSV = 1.2 h^{-1}, and H_2/feed volume ratio = 267 m^3/m^3.

Fig. 4b records when the reaction time was increased to 25 h the BTX selectivities are in the following order: 5%Zr/ZSM-5 ˃ H-ZSM-5 ˃ 5%Ni/ZSM-5 ˃ 5%Nb/ZSM-5 ≈ 5%Ga/ZSM-5 ˃ 20%W/ZSM-5 ˃ 20%Zr/ZSM-5 ˃ 20%$H_3[P(W_3O_{10})_4]$/ZSM-5 ˃ 5%Sn/ZSM-5 ˃ 2.5%Ni2.5%Mo/ZSM-5. These results indicate that the 5%Zr/ZSM-5 is a slightly more selective and stable catalyst than the parent H-ZSM-5 within a longer reaction time, which is also corroborated by the analysis of carbon content in the spent catalysts. The higher selectivity of the 5%Zr/ZSM-5 catalyst can be attributed to the higher amount of the strong BAS. It is noteworthy that 2.5%Ni2.5%Mo/ZSM-5 catalyst shows complete tetralin conversion, mainly into gas products even after 25 h.

Fig. 5a displays the selectivity of gas and liquid in the product mixture after tetralin conversion under ambient pressure. It is evident that the most active catalysts generate a high amount of gas fraction in the following order 2.5%Ni2.5%Mo/ZSM-5 › 5%Zr/ZSM-5 › H-ZSM-5 › 5%Nb/ZSM-5 ≈ 5%Sn/ZSM-5 › 20%Zr/ZSM-5 › 5%Ni/ZSM-5 › 20%W/ZSM-5 › 20%$H_3[P(W_3O_{10})_4]$/ZSM-5 › 5%Ga/ZSM-5. Fig. 5b illustrates that all the catalyst samples (excluding 2.5%Ni2.5%Mo/ZSM-5) show a significant decreasing of the gas products amount (<20 wt%) with increasing the reaction time, while the liquid fraction was ≥80 wt%. This fact can be related to the catalyst deactivation after a longer reaction time. The absence of liquid fraction and increased gaseous fraction yield over the 2.5%Ni2.5%Mo/ZSM-5 catalyst is caused by overcracking. We speculate that the main reason for the overcracking of tetralin into gaseous products over 2.5%Ni2.5%Mo/ZSM-5 catalyst can be attributed to the synergistic effect between Ni and Mo [62]. Interestingly, we have observed a similar effect (overcracking) when naphthalene and 1-methylnaphthalene feedstock mixture was utilized in our

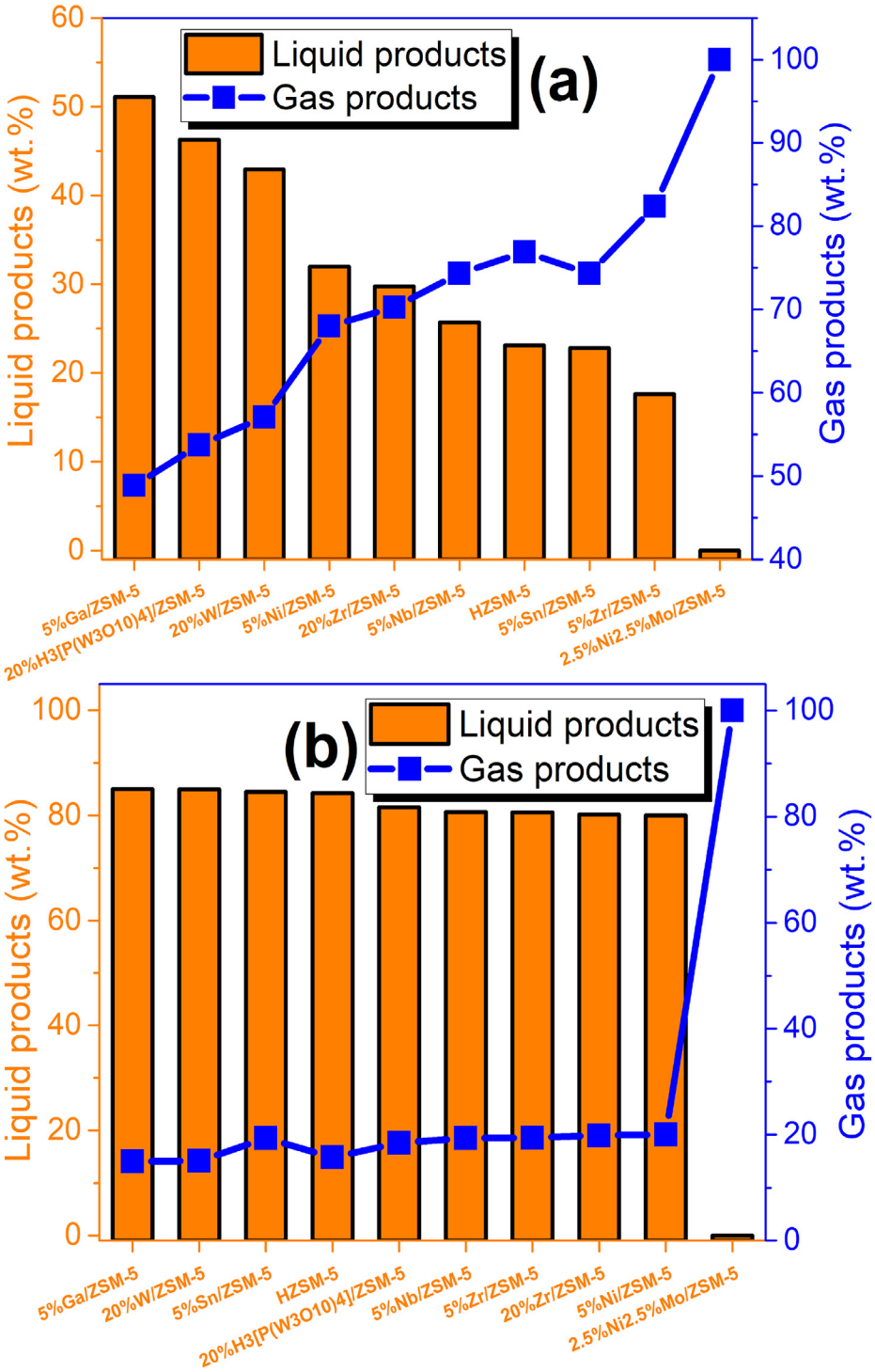

Fig. 5. Selectivity of gas and liquid in products of tetralin hydrocracking over pristine HZSM-5 and metal(s)-modified catalysts with TOS = 4 h – (a) and TOS = 25 h – (b). Rxn conditions: catalyst, 0.5 g; $T_{reactor}$ = 370 °C; H_2 carrier gas; $WHSV_{Tetralin}$ = 2 h^{-1}; $GHSV_{total}$ = 980 h^{-1}; H_2/Tetralin = 1800 (volume ratio); P = 1 bar.

previous paper [13]. Among all studied NiMo-promoted (H-Beta, H-Mordenite, H-USY, H–Y, and H-ZSM-5) catalysts, the 2.5Ni2.5Mo/ZSM-5 exhibited the highest ability to overcracking of polycyclic aromatic hydrocarbons (PAHs). When the 5%Ni/ZSM-5 catalyst was studied the amount of liquid products increased and gaseous products (ethylene and propane) decreased compared to 2.5Ni2.5Mo/ZSM-5 catalyst under the same reaction conditions [14]. We can assume that this behavior is attributed to the difference in the structural and textural characteristics.

According to the literature [63–65], the introduction of Mo into Ni/ZSM-5 can affect the anti-sintering of Ni (prevent the growth of Ni particles), increase hydrocracking activity (in our case we observed overcracking), increase the interaction between Ni species and support, and reduce the amount of carbon deposition. Indeed, it can be seen in our study (Fig. 11) the lowest amount of carbon was observed over the 2.5%Ni2.5%Mo/ZSM-5 catalyst. On the other hand, adding only Ni atom to ZSM-5 support can inhibit overcracking and thus reduce the amount of gaseous products [66].

The gas-phase product distribution over studied catalysts is presented in Fig. 6. It can be seen that ethylene and propane are the main gas products over all the studied catalysts with TOS = 4 h, excluding the 5%Ga/ZSM-5, 20%HPA/ZSM-5, 5%Ni/ZSM-5, and 2.5% Ni2.5%Mo/ZSM-5 catalysts (Fig. 6a). It is worth noting that the presence of Ni species in the 5%Ni/ZSM-5 and 2.5%Ni2.5%Mo/ZSM-5 samples caused a generation of CH_4 as the primary gas product in the gas mixture. This result can be attributed to the high hydrogenolysis and methanation activity of Ni species incorporated into the zeolite framework [67]. For instance, the Ribeiro group [68,69] demonstrated that over Ni-based zeolite catalysts it is possible to achieve a high level of CO_2 conversion and CH_4 selectivity. In addition, Hart et al. [70] observed CH_4 formation, as the main gas product, in the naphthalene hydrogenation and tetralin dehydrogenation reactions over $NiMo/Al_2O_3$ catalyst at 300 °C under 18 bar. Interestingly, the formation of a high amount of CH_4 in our study was also observed over the 5%Ga/ZSM-5 catalyst, which can be related to transfer-de (hydrogenation) reactions enabled by Ga species [71].

When the reactions were carried out for 25 h (Fig. 6b) the gas phase product distribution was not significantly altered compared to TOS = 4 h. Only the 20%HPA/ZSM-5 catalyst exhibited a high amount of ethane and propane at 4 and 25 h, respectively. The possible presence of a high amount of ethane and propane in the gas mixture, after hydrogenation and dehydrogenation of tetralin and naphthalene, was confirmed in the literature [70]. While the 5%Ga/ZSM-5 catalyst showed only ethylene without the presence of methane after 25 h. This phenomenon can be attributed to the deactivation of the catalyst due to coking, which leads to the deactivation of some active sites responsible for the selectivity of some gas products.

3.3. The effect of temperature on the product distribution

Fig. 7a and b display the effect of reaction temperature on BTX selectivity and tetralin conversion where the 20%W/ZSM-5 catalyst was selected as an example for catalytic testing. It can be observed that increasing the reaction temperature from 320 to 420 °C led to significantly enhanced both tetralin conversion and BTX selectivity. Fig. 7c shows the comparison of BTX yield between the 20%W/ZSM-5 and H-ZSM-5 catalysts. It can be seen that the parent H-ZSM-5 zeolite exhibits the highest BTX yield (43.1%) at TOS = 4 h. While after 25 h the BTX yield significantly dropped (due to coke formation) for both catalysts with similar results: H-ZSM-5 – 7.2% and 20%W/ZSM-5 – 7.8%.

As an example, the gas product distributions over the 20%W/ZSM-5 catalyst at different reaction temperatures (from 320 to 420 °C) and TOS (4 and 25 h) are presented in Fig. 8. It is worth mentioning that the amount of gas products significantly depends on the reaction temperature, while the time-on-stream has no significant effect on the latter. Ethylene, propane, and ethane gas products were detected. Notably, the amount of ethylene significantly increased when the reaction temperature increased from 320 to 420 °C, while the amount of propane decreased. According to Corma et al. [72], a large amount of ethylene can be obtained after decalin cracking over the ZSM-5 catalyst at 450 °C. The formation of the high amount of ethylene at high temperature was explained by unimolecular reactions which involve the β-scission of the alkynaphthene carbenium ion and isomerization reactions.

Fig. 9 shows the proposed reaction pathway based on the obtained experimental results of tetralin conversion over H-ZSM-5 catalyst under ambient pressure. It was found that BTX mixture is the main reaction product in the liquid phase, while indane, *trans*-decalin, *cis*-decalin, naphthalene, 2-methylnaphthalene, and 1-methylnaphthalene are the main byproducts. This sequence (Fig. 9) demonstrated that *trans*-decalin and *cis*-decalin were obtained after hydrogenation of tetralin, while indane through the isomerization (ring contraction) reaction. Naphthalene most probably appeared as a result of tetralin dehydrogenation, hydrogen transfer (between feedstock and the adsorbed carbenium ions), and/or bimolecular reactions of two tetralin molecules [73,74]. 1-methylnaphthalene is formed from naphthalene after alkylation (transalkylation) reaction of the latter related to the bimolecular disproportionation reactions what is supported by the studies of Corma et al. [72]. 2-methylnaphthtalne was detected as a result of isomerization of 1-methylnaphthalene. This was studied in detail in our previous publications [13–15]. The gas products such as ethylene, propane, ethane, and methane were detected as a result of overcracking and can be explained by unimolecular reactions [72]. According to the literature [72,73], we can assume that hydrocracking of tetralin into BTX over H-ZSM-5 catalyst is carried out on the BAS of the zeolite with the formation of carbenium and carbenium ions related to an unimolecular mechanism which leads to β-scission and protolytic cracking of ring opening products.

Fig. 10 illustrates the comparison of the most active zeolite supported catalysts from the literature [20–24] to H-ZSM-5 studied in our reaction conditions. It can be seen that H-ZSM-5 catalyst in our study has an advantage due to the fact that the reaction was carried out under atmospheric pressure and relatively mild reaction temperature (420 °C), while catalyst samples from other references were studied under high pressure (40–80 bar) in the temperature range of 370–550 °C. At the same time, the BTX yield achieved over H-ZSM-5 catalyst in our reaction conditions has no significant difference compared to the literature data.

The catalytic behaviours of bifunctional metal-modified ZSM-5 catalysts are significantly influenced by the interaction of the two functional components (metal species and zeolite), and the extent of influence is dependent on the type of metal species added [50]. It was found that Zr migration promoted the reaction process towards BTX formation over 5%Zr/ZSM-5. Considering the synergy between metal oxides and ZSM-5 zeolite, the complex relationship between physicochemical properties and catalytic activity for bifunctional catalyst was detected. The introduction of metal species can influence the acid properties, steric effect, diffusion effect, and specific surface area which lead to the change of the SiO_2/Al_2O_3 ratio, pore size, and particle size and thus alter the catalytic performance [75].

Based on the obtained physicochemical characterization of the catalyst samples we can assume that the combination of catalyst acidity, pore size, particle size, and metal dispersion (location of metal species) in the zeolite matrix in ZSM-5-supported catalysts have a significant effect on the conversion of tetralin and BTX selectivity. The connection between catalyst activity and acidic/textural characteristics is complex and can not be expressed

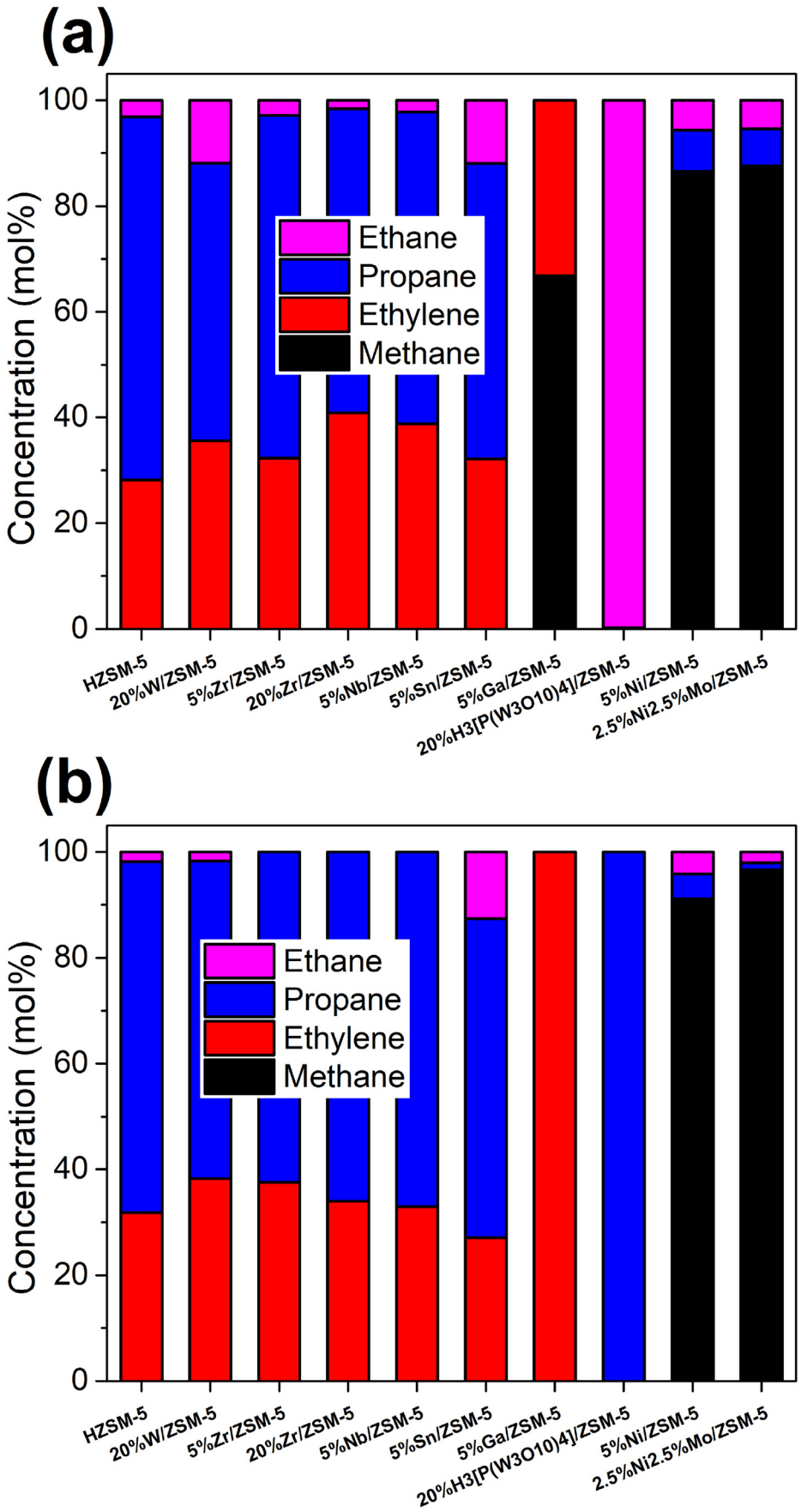

Fig. 6. Gas phase product distribution over pristine H-ZSM-5 and metal(s)-modified zeolite catalysts with TOS = 4 h – (a) and TOS = 25 h – (b). Rxn conditions: catalyst, 0.5 g; $T_{reactor}$ = 370 °C; H_2 carrier gas; $WHSV_{Tetralin}$ = 2 h^{-1}; $GHSV_{total}$ = 980 h^{-1}; H_2/Tetralin = 1800 (volume ratio); P = 1 bar.

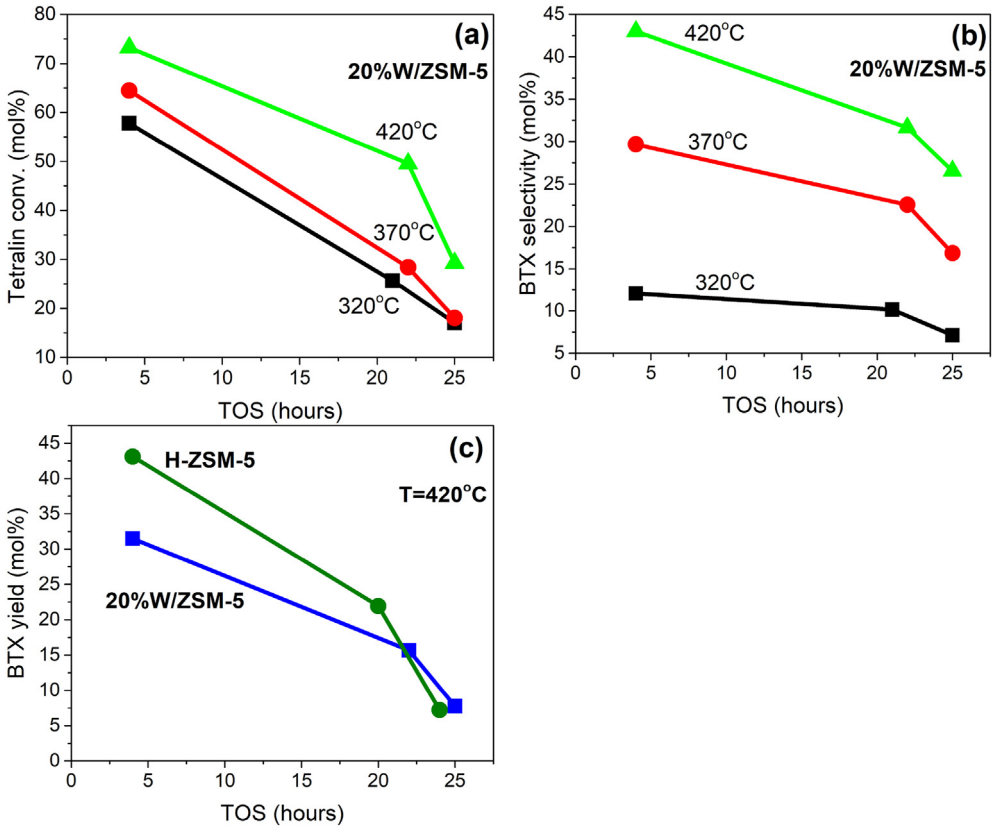

Fig. 7. Tetralin conversion – (a), BTX selectivity – (b) over 20%W/ZSM-5 catalyst at 320, 370, and 420 °C within time-on-stream and BTX yield comparison between H-ZSM-5 and 20%W/ZSM-5 catalysts at 420 °C – (c). Rxn conditions: catalyst, 0.5 g; H_2 carrier gas; $WHSV_{Tetralin} = 2\ h^{-1}$; $GHSV_{total} = 980\ h^{-1}$; H_2/Tetralin = 1800 (volume ratio); P = 1 bar.

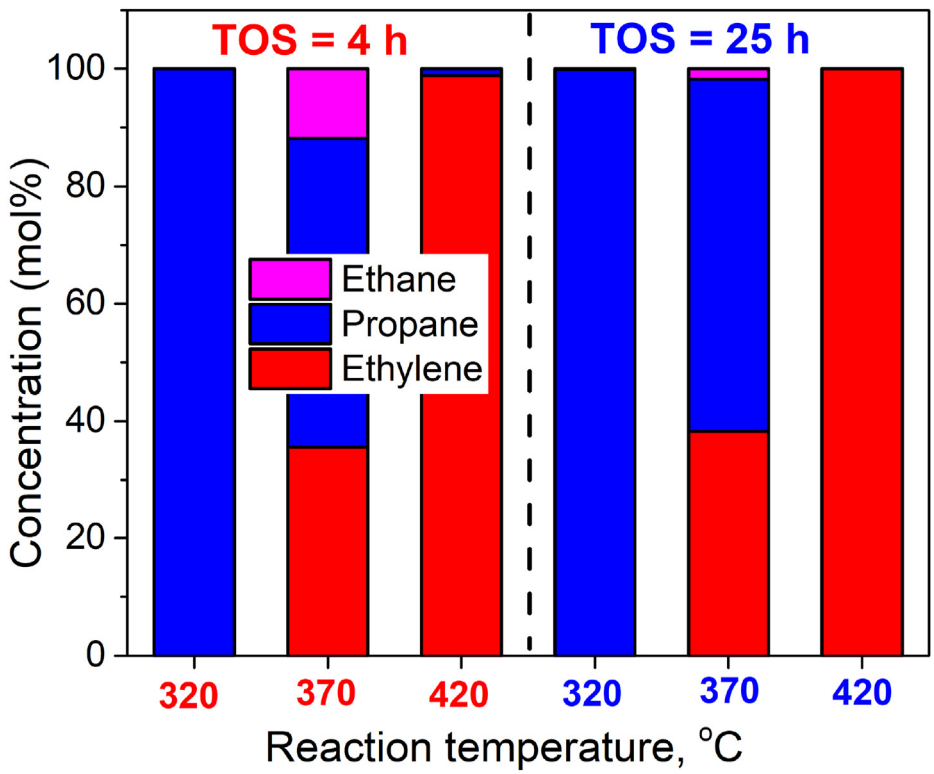

Fig. 8. Gas phase product distribution at 320, 370, and 420 °C over the 20%W/ZSM-5 catalyst. Rxn conditions: catalyst, 0.5 g; H_2 carrier gas; $WHSV_{Tetralin} = 2\ h^{-1}$; $GHSV_{total} = 980\ h^{-1}$; H_2/Tetralin = 1800 (volume ratio); P = 1 bar.

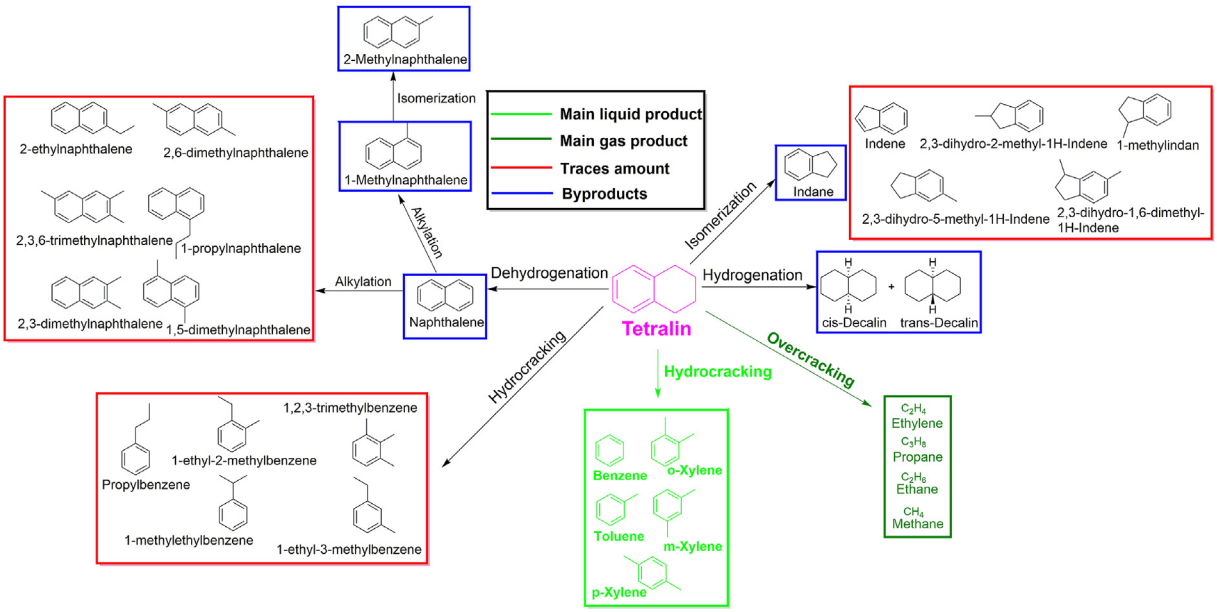

Fig. 9. Proposed reaction pathway of tetralin conversion into value-added BTX products over H-ZSM-5 catalyst under atmospheric pressure.

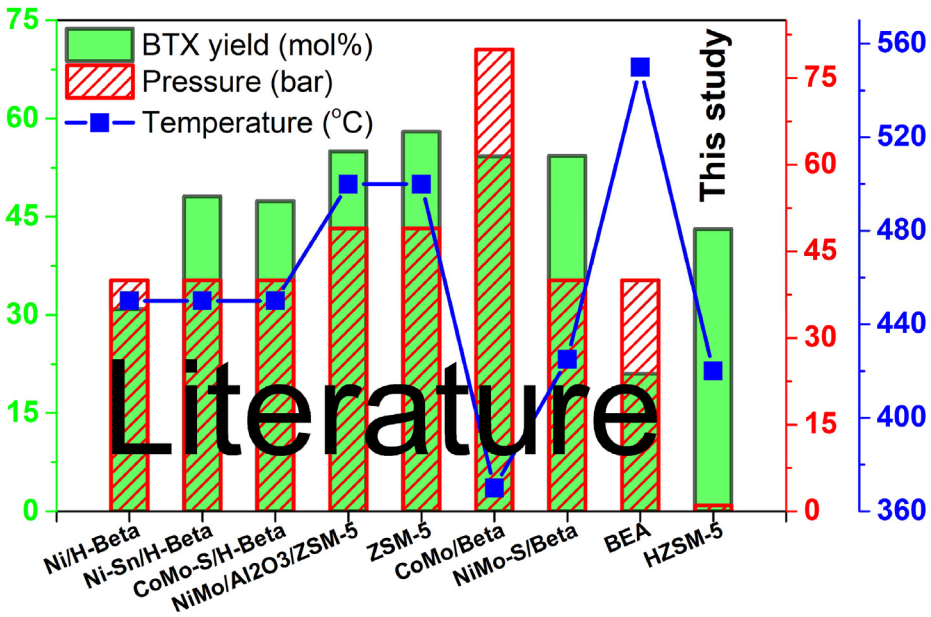

Fig. 10. Comparison of the literature results [20–24] and the studied the most active H-ZSM-5 catalyst in the hydrocracking of tetralin under different reaction temperatures and pressures.

straightforwardly via dependence in one figure. According to obtained experimental results, there is no perfect correlation between all structural and acid properties of studied catalysts and total conversion but we strongly believe that a combination of the suitable acidity with a high amount of strong BAS content, BAS/LAS ratio, and specific surface area play crucial roles for the high catalytic performance in the reaction of conversion of tetralin to BTX. We suppose there exist a global optimum where all of the above mentioned parameters are perfectly balanced but unfortunately, it is complicated to prepare the exact catalyst by controlling all of these optimal parameters. The 5%Zr/ZSM-5 catalyst is probably closer to the optimal values than other metal-loaded zeolite catalysts.

3.4. Catalyst deactivation and regeneration

The amount of coke was quantified for the spent catalysts by total carbon (TC) analysis and compared with each other after the same reaction conditions. Fig. 11 shows that the resistance to carbon deposition decreased as follows 2.5%Ni2.5%Mo/ZSM-5 > 20%W/ZSM-5 > 5%Ni/ZSM-5 > 20%$H_3[P(W_3O_{10})_4]$/ZSM-5 > 5%Nb/ZSM-5 > 5%Ga/ZSM-5 > 5%Sn/ZSM-5 > 20%Zr/ZSM-5 > 5%Zr/ZSM-5 > H-ZSM-5. It reveals that pristine H-ZSM-5 zeolite possessed the highest amount of coke – 5.9 wt%. This observation can be attributed to the highest amount of BAS, which is responsible for the coke formation. When metals were impregnated to zeolite framework the Brønsted acidic protons (Si–OH–Al) were replaced by metal cation(s), which led to

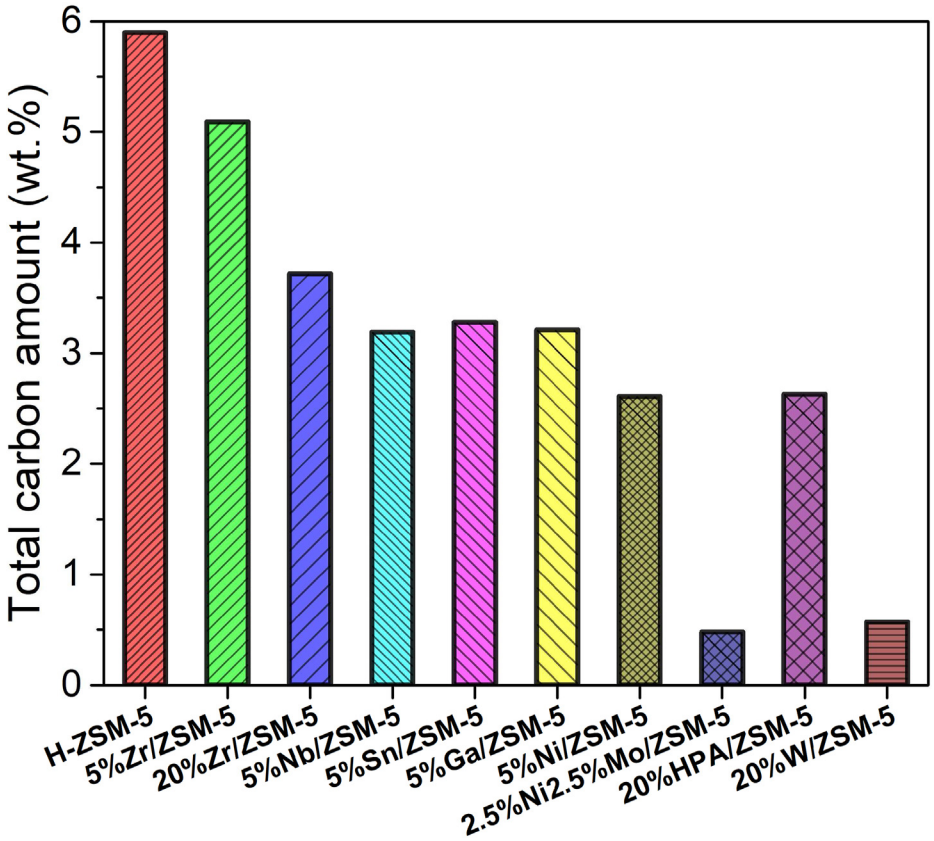

Fig. 11. The total carbon amount in the spent catalysts. Rxn conditions: catalyst, 0.5 g; $T_{reactor}$ = 370 °C; TOS = 25 h; H_2 carrier gas; $WHSV_{Tetralin}$ = 2 h^{-1}; $GHSV_{total}$ = 980 h^{-1}; H_2/Tetralin = 1800 (volume ratio); P = 1 bar.

the decrease of BAS and increase of LAS amount [76].

After metal impregnation, only the 5%Zr/ZSM-5 catalysts exhibited the highest coke deposition (5.1 wt%) among other metal impregnated catalysts. This result can be attributed to higher total acidity and activity of the catalyst with a higher amount of BTX products formed, which leads to enhanced coke deposition. Interestingly, the 20%Zr/ZSM-5 is the next catalyst sample with a high carbon amount. This phenomenon can be related to the low thermomigration ability of Zr, which leaves some of BAS unoccupied, which in turn leads to the high coke formation.

In our previous work [6] we have found that spent H-ZSM-5 catalyst is able to be completely regenerated after treatment in the air atmosphere at 550 °C for 6 h. It was found, by XRD analysis, that after coke deposition the crystalline structure of H-ZSM-5 catalyst is reversed from tetragonal to the orthorhombic one, which indicates a complete catalyst recovery.

We suppose that metal(s) impregnation blocked ZSM-5 domains resulting in the reduced accessibility and activity of the latter, which leads to a decrease in coke formation and changes the morphology of the catalyst and thus, alters its catalytic performance. This observation is in agreement with a study recently published by the Weckhuysen group [77], where zeolite Y catalysts with depositions of Fe, Ni, and V were investigated in the industrial Fluid Catalytic Cracking (FCC) operation of polypropylene aromatization. The authors found that the strong acidity of the zeolite material and the related micropore structure are not necessary for the high aromatic selectivity, while the coke deposition resistance over catalysts with deposited metals was increased compared to the catalysts without metals adding.

Thus, the catalyst with high accessibility and strength of the acid sites together with the optimal balance between micro- and mesopores is essential to achieve the high catalytic performance for BTX production from tetralin under ambient pressure.

4. Conclusions

Herein, we studied and compared various metal(s)-modified H-ZSM-5 zeolite catalysts without sulfidation procedures in the reaction of tetralin (as a biomass tar model compound) hydrocracking into BTX main products under ambient pressure. The BTX selectivity decreases in the order: H-ZSM-5 ˃ 5%Zr/ZSM-5 ˃ 5%Nb/ZSM-5 ˃ 20%W/ZSM-5 ˃ 5%Ni/ZSM-5 ˃ 20%Zr/ZSM-5 ˃ 20%$H_3[P(W_3O_{10})_4]$/ZSM-5 ˃ 5%Sn/ZSM-5 ˃ 5%Ga/ZSM-5 ˃ 2.5%Ni2.5%Mo/ZSM-5. The highest BTX selectivity at 45.6% and tetralin conversion at 94.6% were achieved over the H-ZSM-5 catalyst at 420 °C after 4 h time-on-stream. At the same time, the 5%Zr/ZSM-5 catalyst shows the highest selectivity, with S_{BTX} = 24.2% after 25 h on stream at 370 °C, which can be attributed to the low zirconium species migration between oxide and H-ZSM-5 zeolite framework. The 5%Zr/ZSM-5 catalyst was not optimized but exhibited promising activity and BTX selectivity results. Considering the synergy between metal oxides and ZSM-5 zeolite, the complex relationship between physicochemical properties and catalytic activity for bifunctional catalyst was detected. We demonstrate that high dealkylation activity, mesoporous structure, and the suitable acidity of the ZSM-5 pristine zeolite with a high amount of strong Brønsted acid sites content, BAS/LAS ratio, and specific surface area play crucial roles in tuning the product selectivity of BTX formation. The reaction pathway of BTX production from tetralin is mostly related to the unimolecular mechanism with β-scission and protolytic cracking.

These results are an important step towards developing and designing high-performance catalysts for BTX production from biomass tar or PAHs under ambient pressure.

CRediT authorship contribution statement

Andrii Kostyniuk: Conceptualization, Methodology, Investigation, Formal analysis, Writing – original draft, preparation, Writing – review &amp editing, Data curation, Visualization, Project administration. **David Bajec:** Writing – review &amp editing. **Blaž Likozar:** Supervision, Resources, Conceptualization, Funding acquisition, Project administration.

Declaration of competing interest

The authors declare that they have no known competing financial interests or personal relationships that could have appeared to influence the work reported in this paper.

Acknowledgements

The authors acknowledge financial support from the EU Framework Programme for Research and Innovation Horizon 2020 under Grant Agreement No. 818135 (CONVERGE) and from the Slovenian Research Agency (research core funding No. P2-0152, J2-2492, J2-1723, and J7-1816). The authors are also thankful to Urška Kavčič for N_2 physisorption measurements and Mr. Edi Kranjc for XRD measurements.

Appendix A. Supplementary data

Supplementary data to this article can be found online at https://doi.org/10.1016/j.renene.2022.01.090.

References

[1] A. Corma, Preface to special issue of ChemSusChem on green carbon science: CO2 capture and conversion, ChemSusChem (2020) 6054–6055, https://doi.org/10.1002/cssc.202002323.
[2] Q. Lin, S. Zhang, J. Wang, H. Yin, Synthesis of modified char-supported Ni–Fe catalyst with hierarchical structure for catalytic cracking of biomass tar, Renew. Energy 174 (2021) 188–198, https://doi.org/10.1016/j.renene.2021.04.084.
[3] Y. Shen, Y. Fu, Advances in: in situ and ex situ tar reforming with biochar catalysts for clean energy production, Sustain. Energy Fuels 2 (2018) 326–344, https://doi.org/10.1039/c7se00553a.
[4] C.P. Jiménez-Gómez, J.A. Cecilia, C. García-Sancho, R. Moreno-Tost, P. Maireles-Torres, Selective production of furan from gas-phase furfural decarbonylation on Ni-MgO catalysts, ACS Sustain. Chem. Eng. 7 (2019) 7676–7685, https://doi.org/10.1021/acssuschemeng.8b06155.
[5] S. Dokjampa, T. Rirksomboon, S. Osuwan, S. Jongpatiwut, D.E. Resasco, Comparative study of the hydrogenation of tetralin on supported Ni, Pt, and Pd catalysts, Catal. Today 123 (2007) 218–223, https://doi.org/10.1016/j.cattod.2007.01.004.
[6] A. Kostyniuk, D. Bajec, B. Likozar, Catalytic hydrocracking reactions of tetralin as aromatic biomass tar model compound to benzene/toluene/xylenes (BTX) over zeolites under ambient pressure conditions, J. Ind. Eng. Chem. 96 (2021) 130–143, https://doi.org/10.1016/j.jiec.2021.01.010.
[7] J. Il Park, J.K. Lee, J. Miyawaki, Y.K. Kim, S.H. Yoon, I. Mochida, Hydro-conversion of 1-methyl naphthalene into (alkyl)benzenes over alumina-coated USY zeolite-supported NiMoS catalysts, Fuel 90 (2011) 182–189, https://doi.org/10.1016/j.fuel.2010.09.002.
[8] Y.S. Kim, G.N. Yun, Y.K. Lee, Novel Ni2P/zeolite catalysts for naphthalene hydrocracking to BTX, Catal. Commun. 45 (2014) 133–138, https://doi.org/10.1016/j.catcom.2013.11.010.
[9] T. Wu, S.L. Chen, G.M. Yuan, X. Pan, J. Du, Y. Zhang, N. Zhang, High metal-acid balance and selective hydrogenation activity catalysts for hydrocracking of 1-methylnaphthalene to benzene, toluene, and xylene, Ind. Eng. Chem. Res. 59 (2020) 5546–5556, https://doi.org/10.1021/acs.iecr.9b06158.
[10] R. Michel, A. Łamacz, A. Krzton, G. Djéga-Mariadassou, P. Burg, C. Courson, R. Gruber, Steam reforming of α-methylnaphthalene as a model tar compound over olivine and olivine supported nickel, Fuel 109 (2013) 653–660, https://doi.org/10.1016/j.fuel.2013.03.017.
[11] K. Qian, A. Kumar, Catalytic reforming of toluene and naphthalene (model tar) by char supported nickel catalyst, Fuel 187 (2017) 128–136, https://doi.org/10.1016/j.fuel.2016.09.043.
[12] A. Veksha, A. Giannis, W. Da Oh, V.W.C. Chang, G. Lisak, T.T. Lim, Catalytic activities and resistance to HCl poisoning of Ni-based catalysts during steam reforming of naphthalene, Appl. Catal. Gen. 557 (2018) 25–38, https://doi.org/10.1016/j.apcata.2018.03.005.
[13] A. Kostyniuk, D. Bajec, B. Likozar, Hydrocracking, hydrogenation and isomerization of model biomass tar in a packed bed reactor over bimetallic NiMo zeolite catalysts: tailoring structure/acidity, Appl. Catal. Gen. 612 (2021) 118004, https://doi.org/10.1016/j.apcata.2021.118004.
[14] A. Kostyniuk, D. Bajec, B. Likozar, Catalytic hydrogenation, hydrocracking and isomerization reactions of biomass tar model compound mixture over Ni-modified zeolite catalysts in packed bed reactor, Renew. Energy 167 (2021) 409–424, https://doi.org/10.1016/j.renene.2020.11.098.
[15] A. Kostyniuk, D. Bajec, A. Praśnikar, B. Likozar, Catalytic hydrocracking, hydrogenation, and isomerization reactions of model biomass tar over (W/Ni)-zeolites, J. Ind. Eng. Chem. 101 (2021) 293–306, https://doi.org/10.1016/j.jiec.2021.06.001.
[16] BTX (Benzene Toluene and Xylene) Market, 2020, p. 150. https://www.reportsanddata.com/report-detail/btx-benzene-toluene-and-xylene-market.
[17] F. Wang, W. Xiao, L. Gao, G. Xiao, Enhanced performance of glycerol to aromatics over Sn-containing HZSM-5 zeolites, RSC Adv. 6 (2016) 42984–42993, https://doi.org/10.1039/C6RA03358J.
[18] D. Kiani, S. Sourav, Y. Tang, J. Baltrusaitis, I.E. Wachs, Methane activation by ZSM-5-supported transition metal centers, Chem. Soc. Rev. 50 (2021) 1251–1268, https://doi.org/10.1039/d0cs01016b.
[19] Q. Che, M. Yang, X. Wang, Q. Yang, L. Rose Williams, H. Yang, J. Zou, K. Zeng, Y. Zhu, Y. Chen, H. Chen, Influence of physicochemical properties of metal modified ZSM-5 catalyst on benzene, toluene and xylene production from biomass catalytic pyrolysis, Bioresour. Technol. 278 (2019) 248–254, https://doi.org/10.1016/j.biortech.2019.01.081.
[20] J. Lee, Y. Choi, J. Shin, J.K. Lee, Selective hydrocracking of tetralin for light aromatic hydrocarbons, Catal. Today 265 (2016) 144–153, https://doi.org/10.1016/j.cattod.2015.09.046.
[21] G.C. Laredo, P. Pérez, R. Pedro, M.V. Merino, E. Arzate, A. García, L. Ricardo, A. Rangel, V.H. Martínez, Effect of the catalytic system and operating conditions on BTX formation using tetralin as a model molecule, Appl. Petrochemical Res. 9 (2019) 185–198, https://doi.org/10.1007/s13203-019-00237-4.
[22] D.P. Upare, S. Park, M.S. Kim, J. Kim, D. Lee, J. Lee, H. Chang, W. Choi, S. Choi, Y.P. Jeon, Y.K. Park, C.W. Lee, Cobalt promoted Mo/beta zeolite for selective hydrocracking of tetralin and pyrolysis fuel oil into monocyclic aromatic hydrocarbons, J. Ind. Eng. Chem. 35 (2016) 99–107, https://doi.org/10.1016/j.jiec.2015.12.020.
[23] J. Shin, Y. Oh, Y. Choi, J. Lee, J.K. Lee, Design of selective hydrocracking catalysts for BTX production from diesel-boiling-range polycyclic aromatic hydrocarbons, Appl. Catal. Gen. 547 (2017) 12–21, https://doi.org/10.1016/j.apcata.2017.08.019.
[24] K. Nakajima, S. Suganuma, E. Tsuji, N. Katada, Mechanism of tetralin conversion on zeolites for the production of benzene derivatives, React. Chem. Eng. 5 (2020) 1272–1280, https://doi.org/10.1039/d0re00128g.
[25] G.C. Laredo, J.L. García-Gutiérrez, P. Pérez-Romo, E.H. Olmos-Cerda, Effect of the catalyst in the BTX production by hydrocracking of light cycle oil, Appl. Petrochemical Res. 11 (2021) 19–38, https://doi.org/10.1007/s13203-021-00266-y.
[26] Y. Choi, J. Lee, J. Shin, S. Lee, D. Kim, J.K. Lee, Selective hydroconversion of naphthalenes into light alkyl-aromatic hydrocarbons, Appl. Catal. Gen. 492 (2015) 140–150, https://doi.org/10.1016/j.apcata.2014.12.001.
[27] P. Bi, Y. Yuan, M. Fan, P. Jiang, Q. Zhai, Q. Li, Production of aromatics through current-enhanced catalytic conversion of bio-oil tar, Bioresour. Technol. 136 (2013) 222–229, https://doi.org/10.1016/j.biortech.2013.02.100.
[28] J. Il Park, S.A. Ali, K. Alhooshani, N. Azizi, J. Miyawaki, T. Kim, Y. Lee, H.S. Kim, S.H. Yoon, I. Mochida, Mild hydrocracking of 1-methyl naphthalene (1-MN) over alumina modified zeolite, J. Ind. Eng. Chem. 19 (2013) 627–632, https://doi.org/10.1016/j.jiec.2012.09.014.
[29] S.U. Lee, Y.J. Lee, J.R. Kim, S.Y. Jeong, Rational synthesis of silylated Beta zeolites and selective ring opening of 1-methylnaphthalene over the NiW-supported catalysts, Appl. Catal. B Environ. 219 (2017) 1–9, https://doi.org/10.1016/j.apcatb.2017.07.047.
[30] S.U. Lee, Y.J. Lee, J.R. Kim, S.Y. Jeong, Tactical control of Ni-loading over W-supported Beta zeolite catalyst for selective ring opening of 1-methylnaphthalene, J. Ind. Eng. Chem. 66 (2018) 279–287, https://doi.org/10.1016/j.jiec.2018.05.042.
[31] Y.S. Kim, K.S. Cho, Y.K. Lee, Morphology effect of b-zeolite supports for Ni2P catalysts on the hydrocracking of polycyclic aromatic hydrocarbons to benzene, toluene, and xylene, J. Catal. 351 (2017) 67–78, https://doi.org/10.1016/j.jcat.2017.03.006.
[32] T. Wu, S.-L. Chen, G. mei Yuan, J. Xu, L. Huang, Y. Cao, T. Fan, High-selective-hydrogenation activity of W/Beta catalyst in hydrocracking of 1-methylnaphalene to benzene, toluene and xylene, Fuel 234 (2018) 1015–1025, https://doi.org/10.1016/j.fuel.2018.07.133.
[33] A. Ishihara, T. Itoh, H. Nasu, T. Hashimoto, T. Doi, Hydrocracking of 1-methylnaphthalene/decahydronaphthalene mixture catalyzed by zeolite-alumina composite supported NiMo catalysts, Fuel Process. Technol. 116 (2013) 222–227, https://doi.org/10.1016/j.fuproc.2013.07.001.

[34] S.U. Lee, Y.J. Lee, J.R. Kim, E.S. Kim, T.W. Kim, H.J. Kim, C.U. Kim, S.Y. Jeong, Selective ring opening of phenanthrene over NiW-supported mesoporous HY zeolite catalyst depending on their mesoporosity, Mater. Res. Bull. 96 (2017) 149–154, https://doi.org/10.1016/j.materresbull.2017.05.002.
[35] Y.P. Wijaya, H.P. Winoto, Y.K. Park, D.J. Suh, H. Lee, J.M. Ha, J. Jae, Heteropolyacid catalysts for Diels-Alder cycloaddition of 2,5-dimethylfuran and ethylene to renewable p-xylene, Catal. Today 293–294 (2017) 167–175, https://doi.org/10.1016/j.cattod.2016.12.032.
[36] R.M. Ladera, J.L.G. Fierro, M. Ojeda, S. Rojas, TiO2-supported heteropoly acids for low-temperature synthesis of dimethyl ether from methanol, J. Catal. 312 (2014) 195–203, https://doi.org/10.1016/j.jcat.2014.01.016.
[37] K. Zhu, J. Hu, X. She, J. Liu, Z. Nie, Y. Wang, C.H.F. Peden, H.K. Ja, Characterization of dispersed heteropoly acid on mesoporous zeolite using solid-state31P NMR spin-lattice relaxation, J. Am. Chem. Soc. 131 (2009) 9715–9721, https://doi.org/10.1021/ja901317r.
[38] X. Su, W. Zan, X. Bai, G. Wang, W. Wu, Synthesis of microscale and nanoscale ZSM-5 zeolites: effect of particle size and acidity of Zn modified ZSM-5 zeolites on aromatization performance, Catal. Sci. Technol. 7 (2017) 1943–1952, https://doi.org/10.1039/c7cy00435d.
[39] T. Wang, C. Yang, P. Gao, S. Zhou, S. Li, H. Wang, Y. Sun, ZnZrOx integrated with chain-like nanocrystal HZSM-5 as efficient catalysts for aromatics synthesis from CO2 hydrogenation, Appl. Catal. B Environ. 286 (2021) 119929, https://doi.org/10.1016/j.apcatb.2021.119929.
[40] S. Vichaphund, D. Aht-Ong, V. Sricharoenchaikul, D. Atong, Production of aromatic compounds from catalytic fast pyrolysis of Jatropha residues using metal/HZSM-5 prepared by ion-exchange and impregnation methods, Renew. Energy 79 (2015) 28–37, https://doi.org/10.1016/j.renene.2014.10.013.
[41] C. Nishu, M. Li, M.M. Chai, Y. Rahman, M. Li, R. Liu Sarker, Performance of alkali and Ni-modified ZSM-5 during catalytic pyrolysis of extracted hemicellulose from rice straw for the production of aromatic hydrocarbons, Renew. Energy 175 (2021) 936–951, https://doi.org/10.1016/j.renene.2021.05.005.
[42] T.C. Hoff, D.W. Gardner, R. Thilakaratne, K. Wang, T.W. Hansen, R.C. Brown, J.P. Tessonnier, Tailoring ZSM-5 zeolites for the fast pyrolysis of biomass to aromatic hydrocarbons, ChemSusChem 9 (2016) 1473–1482, https://doi.org/10.1002/cssc.201600186.
[43] X. Su, G. Wang, X. Bai, W. Wu, L. Xiao, Y. Fang, J. Zhang, Synthesis of nanosized HZSM-5 zeolites isomorphously substituted by gallium and their catalytic performance in the aromatization, Chem. Eng. J. 293 (2016) 365–375, https://doi.org/10.1016/j.cej.2016.02.088.
[44] A. Kostyniuk, D. Bajec, P. Djinović, B. Likozar, Allyl alcohol production by gas phase conversion reactions of glycerol over bifunctional hierarchical zeolite-supported bi- and tri-metallic catalysts, Chem. Eng. J. 397 (2020) 125430, https://doi.org/10.1016/j.cej.2020.125430.
[45] A. Kostyniuk, D. Bajec, P. Djinović, B. Likozar, One-step synthesis of glycidol from glycerol in a gas-phase packed-bed continuous flow reactor over HZSM-5 zeolite catalysts modified by CsNO3, Chem. Eng. J. 394 (2020) 124945, https://doi.org/10.1016/j.cej.2020.124945.
[46] A. Kostyniuk, D. Key, M. Mdleleni, 1-hexene isomerization over bimetallic M-Mo-ZSM-5 (M: Fe, Co, Ni) zeolite catalysts: effects of transition metals addition on the catalytic performance, J. Energy Inst. 93 (2020) 552–564, https://doi.org/10.1016/j.joei.2019.06.009.
[47] M. Li, Y. Zhou, I.N. Oduro, Y. Fang, Comparative study on the catalytic conversion of methanol and propanal over Ga/ZSM-5, Fuel 168 (2016) 68–75, https://doi.org/10.1016/j.fuel.2015.11.076.
[48] N. Al-Yassir, M.N. Akhtar, K. Ogunronbi, S. Al-Khattaf, Synthesis of stable H-galloaluminosilicate MFI with hierarchical pore architecture by surfactant-mediated base hydrolysis, and their application in propane aromatization, J. Mol. Catal. Chem. 360 (2012) 1–15, https://doi.org/10.1016/j.molcata.2012.04.005.
[49] N. Karanwal, M.G. Sibi, M.K. Khan, A.A. Myint, B.C. Ryu, J.W. Kang, J. Kim, Trimetallic Cu–Ni–Zn/H-ZSM-5 catalyst for the one-pot conversion of levulinic acid to high-yield 1 ,4-pentanediol under mild conditions in an aqueous medium, ACS Catal. 11 (2021) 2846–2864, https://doi.org/10.1021/acscatal.0c04216.
[50] Y. Wang, G. Wang, L.I. van der Wal, K. Cheng, Q. Zhang, K.P. de Jong, Y. Wang, Visualizing element migration over bifunctional metal-zeolite catalysts and its impact on catalysis, Angew. Chem. Int. Ed. (2021) 2–11, https://doi.org/10.1002/anie.202107264.
[51] U.V. Mentzel, K.T. Højholt, M.S. Holm, R. Fehrmann, P. Beato, Conversion of methanol to hydrocarbons over conventional and mesoporous H-ZSM-5 and H-Ga-MFI: major differences in deactivation behavior, Appl. Catal. Gen. 417–418 (2012) 290–297, https://doi.org/10.1016/j.apcata.2012.01.003.
[52] Y. Liao, S.F. Koelewijn, G. van den Bossche, J. van Aelst, S. van den Bosch, T. Renders, K. Navare, T. Nicolaï, K. van Aelst, M. Maesen, H. Matsushima, J.M. Thevelein, K. van Acker, B. Lagrain, D. Verboekend, B.F. Sels, A sustainable wood biorefinery for low-carbon footprint chemicals production, Science 367 (80) (2020) 1385–1390, https://doi.org/10.1126/science.aau1567.
[53] A. Maity, S. Chaudhari, J.J. Titman, V. Polshettiwar, Catalytic nanosponges of acidic aluminosilicates for plastic degradation and CO2 to fuel conversion, Nat. Commun. 11 (2020), https://doi.org/10.1038/s41467-020-17711-6.
[54] Z. Cao, X. Zhang, C. Xu, X. Huang, Z. Wu, C. Peng, A. Duan, Selective hydrocracking of light cycle oil into high-octane gasoline over bi-functional catalysts, J. Energy Chem. 52 (2021) 41–50, https://doi.org/10.1016/j.jechem.2020.04.055.
[55] O.V. Larina, N.D. Shcherban, P.I. Kyriienko, I.M. Remezovskyi, P.S. Yaremov, I. Khalakhan, G. Mali, S.O. Soloviev, S.M. Orlyk, S. Dzwigaj, Design of effective catalysts based on ZnLaZrSi oxide systems for obtaining 1,3-butadiene from aqueous ethanol, ACS Sustain. Chem. Eng. 8 (2020) 16600–16611, https://doi.org/10.1021/acssuschemeng.0c05925.
[56] J. Chen, H. Shi, L. Li, K. Li, Deoxygenation of methyl laurate as a model compound to hydrocarbons on transition metal phosphide catalysts, Appl. Catal. B Environ. 144 (2014) 870–884, https://doi.org/10.1016/j.apcatb.2013.08.026.
[57] R. Buzzoni, S. Bordiga, G. Ricchiardi, C. Lamberti, A. Zecchina, G. Bellussi, Interaction of pyridine with acidic (H-ZSM5, H-β, H-MORD zeolites) and superacidic (H-nafion membrane) systems: an IR investigation, Langmuir 12 (1996) 930–940, https://doi.org/10.1021/la950571i.
[58] C.A. Emeis, Determination of integrated molar extinction coefficients for infrared absorption bands of pyridine adsorbed on solid acid catalysts, J. Catal. 141 (1993) 347–354, https://doi.org/10.1006/jcat.1993.1145.
[59] V.D.O. Rodrigues, A.C. Faro Júnior, On catalyst activation and reaction mechanisms in propane aromatization on Ga/HZSM5 catalysts, Appl. Catal. Gen. 435–436 (2012) 68–77, https://doi.org/10.1016/j.apcata.2012.05.036.
[60] C. Freitas, N.S. Barrow, V. Zholobenko, Accessibility and location of acid sites in zeolites as probed by fourier transform infrared spectroscopy and magic angle spinning nuclear magnetic resonance, Johnson Matthey Technol. Rev. 62 (2018) 279–290, https://doi.org/10.1595/205651318X696792.
[61] N. Kosinov, C. Liu, E.J.M. Hensen, E.A. Pidko, Engineering of transition metal catalysts confined in zeolites, Chem. Mater. 30 (2018) 3177–3198, https://doi.org/10.1021/acs.chemmater.8b01311.
[62] J. Shi, L. Sun, H. Yan, J. Wang, Catalytic hydrotreatment of pine sawdust hydropyrolysis vapor over Ni, Mo-impregnated HZSM-5 for optimal production of gasoline components, Energy Fuel. (2021), https://doi.org/10.1021/acs.energyfuels.1c03271.
[63] J. Zhang, T. Chen, Y. Jiao, M. Cheng, L.-L. Wang, J.-L. Wang, X.-Y. Li, Y.-Q. Chen, Improved activity of Ni–Mo/SiO2 bimetallic catalyst synthesized via sol-gel method for methylcyclohexane cracking, Petrol. Sci. 18 (2021) 1530–1542, https://doi.org/10.1016/j.petsci.2021.08.009.
[64] T. Huang, W. Huang, J. Huang, P. Ji, Methane reforming reaction with carbon dioxide over SBA-15 supported Ni-Mo bimetallic catalysts, Fuel Process. Technol. 92 (2011) 1868–1875, https://doi.org/10.1016/j.fuproc.2011.05.002.
[65] C.E. Quincoces, S.P. De Vargas, P. Grange, M.G. Gonza, Role of Mo in CO2 reforming of CH4 over Mo promoted Ni/Al2O3 catalysts, Mater. Lett. 56 (2002) 698–704.
[66] Q. Wei, P. Zhang, X. Liu, W. Huang, X. Fan, Y. Yan, R. Zhang, L. Wang, Y. Zhou, Synthesis of Ni-modified ZSM-5 zeolites and their catalytic performance in n-octane hydroconversion, Front. Chem. 8 (2020) 1–8, https://doi.org/10.3389/fchem.2020.586445.
[67] N.A. Sholeha, S. Mohamad, H. Bahruji, D. Prasetyoko, N. Widiastuti, N.A. Abdul Fatah, A.A. Jalil, Y.H. Taufiq-Yap, Enhanced CO2methanation at mild temperature on Ni/zeolite from kaolin: effect of metal-support interface, RSC Adv. 11 (2021) 16376–16387, https://doi.org/10.1039/d1ra01014j.
[68] I. Graça, L.V. González, M.C. Bacariza, A. Fernandes, C. Henriques, J.M. Lopes, M.F. Ribeiro, CO2 hydrogenation into CH4 on NiHNaUSY zeolites, Appl. Catal. B Environ. 147 (2014) 101–110, https://doi.org/10.1016/j.apcatb.2013.08.010.
[69] M.C.B.I. Grac, CO2 hydrogenation over Ni-based zeolites: effect of catalysts preparation and pre-reduction conditions on methanation performance, Top. Catal. 59 (2016) 314–325, https://doi.org/10.1007/s11244-015-0435-4.
[70] A. Hart, M. Adam, J.P. Robinson, S.P. Rigby, J. Wood, Hydrogenation and dehydrogenation of tetralin and naphthalene to explore heavy oil upgrading using NiMo/Al2O3 and CoMo/Al2O3 catalysts heated with steel balls via induction, Catalysts 497 (2020) 1–18.
[71] E.A. Uslamin, B. Luna-Murillo, N. Kosinov, P.C.A. Bruijnincx, E.A. Pidko, B.M. Weckhuysen, E.J.M. Hensen, Gallium-promoted HZSM-5 zeolites as efficient catalysts for the aromatization of biomass-derived furans, Chem. Eng. Sci. 198 (2019) 305–316, https://doi.org/10.1016/j.ces.2018.09.023.
[72] A. Corma, V. González-Alfaro, A.V. Orchillés, Decalin and tetralin as probe molecules for cracking and hydrotreating the light cycle oil, J. Catal. 200 (2001) 34–44, https://doi.org/10.1006/jcat.2001.3181.
[73] M. Santikunaporn, J.E. Herrera, S. Jongpatiwut, D.E. Resasco, W.E. Alvarez, E.L. Sughrue, Ring opening of decalin and tetralin on HY and Pt/HY zeolite catalysts, J. Catal. 228 (2004) 100–113, https://doi.org/10.1016/j.jcat.2004.08.030.
[74] R. Bounaceur, G. Scacchi, P.M. Marquaire, F. Dominé, Mechanistic modeling of the thermal cracking of tetralin, Ind. Eng. Chem. Res. 39 (2000) 4152–4165, https://doi.org/10.1021/ie000276f.
[75] D. Liu, L. Cao, G. Zhang, L. Zhao, J. Gao, C. Xu, Catalytic conversion of light alkanes to aromatics by metal-containing HZSM-5 zeolite catalysts—a review, Fuel Process. Technol. 216 (2021) 106770, https://doi.org/10.1016/j.fuproc.2021.106770.
[76] W. Li, K. Wang, G. Zhan, J. Huang, Q. Li, Hydrogenation of CO2 to dimethyl ether over tandem catalysts based on biotemplated hierarchical ZSM-5 and Pd/ZnO, ACS Sustain. Chem. Eng. 8 (2020) 14058–14070, https://doi.org/10.1021/acssuschemeng.0c04399.
[77] I. Vollmer, M.J.F. Jenks, R. Mayorga González, F. Meirer, B.M. Weckhuysen, Plastic waste conversion over a refinery waste catalyst, Angew. Chem. Int. Ed. (2021) 16101–16108, https://doi.org/10.1002/anie.202104110.